Journal of Medicinal Chemistry

Article

Discovery of the Clinical Candidate 2-(4-(2-((1*H*-benzo[*d*]imidazol-2-yl)thio)ethyl)piperazin-1-yl)- *N*-(6-methyl-2,4-bis(methylthio)pyridin-3-yl)acetamide hydrocholoride [K-604], an Aqueous Soluble Acyl-CoA: Cholesterol *O*-Acyltransferase (ACAT/SOAT)-1 Inhibitor

Kimiyuki Shibuya, Katsumi Kawamine, Chiyoka Ozaki, Tadaaki Ohgiya, Toshiyuki Edano, Yasunobu Yoshinaka, and Yoshihiko Tsunenari

J. Med. Chem., **Just Accepted Manuscript** • DOI: 10.1021/acs.jmedchem.8b01256 • Publication Date (Web): 15 Nov 2018

ACS Publications

is published by the American Chemical Society. 1155 Sixteenth Street N.W., Washington, DC 20036

Discovery of the Clinical Candidate 2-(4-(2-((1*H*-benzo[*d*]imidazol-2-yl)thio)ethyl)piperazin-1-yl)-*N*-(6-methyl-2,4-bis(methylthio)pyridin-3-yl)acetamide hydrochloride [K-604], an Aqueous-Soluble Acyl-CoA:Cholesterol *O*-Acyltransferase (ACAT/SOAT)-1 Inhibitor

Kimiyuki Shibuya, Katsumi Kawamine, Chiyoka Ozaki, Tadaaki Ohgiya, Toshiyuki Edano, Yasunobu Yoshinaka, Yoshihiko Tsunenari.*

Tokyo New Drug Research Laboratories, Pharmaceutical Division, Kowa Company, Ltd., 2-17-43, Noguchicho, Higashimurayama, Tokyo 189-0022, Japan

KEYWORDS. acyl-CoA:cholesterol *O*-acyltransferase (ACAT/SOAT), ACAT-1 (aortic ACAT), ACAT-2 (intestinal ACAT), isoform selectivity, cholesteryl esters (CEs), lipid accumulation areas, atherosclerosis, aqueous soluble, well absorbed, adrenal toxicity, well tolerated.

ABSTRACT. K-604 (**2**) (2-(4-(2-((1*H*-benzo[*d*]imidazol-2-yl)thio)ethyl)piperazin-1-yl)-*N*-(6-methyl-2,4-bis(methylthio)pyridin-3-yl)acetamide hydrochloride) has been identified as an aqueous-soluble potent inhibitor of human acyl-coenzyme A:cholesterol *O*-acyltransferase (ACAT, also known as SOAT)-1 and exhibits 229-fold selectivity for human ACAT-1 over human ACAT-2. In our molecular design, the insertion of a piperazine unit in the place of a 6-methylene chain into the linker between the head (pyridylacetamide) and tail (benzimidazole) moieties led to a marked enhancement of the aqueous solubility (up to 19 mg/mL at pH 1.2) and a significant improvement of the oral absorption (the Cmax of **2** was 1100-fold higher than that of **1** in fasted dogs) compared to the previously selected compound **1**. After ensuring the pharmacological effects and safety, we designated **2** as a clinical candidate, named **K-604**. Considering the therapeutic results of ACAT inhibitor in past clinical trials, we believe that **K-604** will be useful for the treatment of incurable diseases involving ACAT-1 overexpression.

Introduction

Acyl-coenzyme A:cholesterol *O*-acyltransferase (ACAT), also known as sterol *O*-acyltransferase (SOAT), has received attention as a promising target for hyperlipidemia and atherosclerosis. ACAT catalyzes the acylation of cholesterol with long-chain fatty acids to afford cholesteryl esters (CEs) and is involved in intestinal absorption of dietary cholesterol, incorporation of hepatic cholesterol into very low-density lipoproteins (VLDLs) and vascular accumulation of cholesterol. [1] Therefore, exciting and intensive research activity in both academia and the industry over the last three decades has produced a large number of ACAT inhibitors as poststatin (a 3-hydroxy-3-methylglutaryl (HMG)-CoA reductase inhibitor) targets; [2-5] however, the beneficial effects of these inhibitors have not been demonstrated in clinical trials. [6-10] Two isoforms of ACAT have been identified in mammals and have been shown to have

different substrate specificities and potential functions. ACAT-1 is ubiquitously expressed in various human tissues, predominantly in human liver (Kupffer cells), macrophage, adrenal gland and brain tissue, whereas ACAT-2 is found in human hepatocytes and intestinal tissue. [11-17] Recently, an ACAT-1 inhibitor was highlighted in the context of drug repositioning (repurposing) for potential application in the treatment of the following diseases: 1) In multiple neurodegenerative diseases, including Alzheimer's disease, [18-22] blocking ACAT-1 provides new benefits, such as clearance of amyloid β (Aβ) peptides and suppression of 24(*S*)-hydroxycholesterol-induced neuronal cell death. 2) In nonalcoholic steatohepatitis (NASH), [23] progression of steatosis and liver inflammation via Kupffer cells activated by high levels of CE is involved in ACAT-1 induction. Therefore, ACAT-1 inhibition may be a new therapeutic target for the treatment of NASH. 3) Increased CE levels are widely known to be associated with breast cancer, leukemia, glioma and prostate cancer. [24-27] P. Saraon and his group have proposed that ACAT-1 expression could serve as a potential prognostic marker for prostate cancer, specifically to differentiate between indolent and aggressive forms of cancer. J. Li et al. demonstrated that ACAT-1 inhibition-induced ER stress led to apoptosis in pancreatic cancer cells. C. Xu and coworkers revealed that ACAT-1 inhibition potentiated the antitumor response of $CD8^+$ T cells by modulating cholesterol metabolism. The researchers also demonstrated that ACAT-1 inhibitors can complement current therapies such as immune checkpoint blockade by acting via a different mechanism. These fascinating trends prompted us to report our discovery of the clinical candidate 2-(4-(2-((1*H*-benzo[*d*]imidazol-2-yl)thio)ethyl)piperazin-1-yl)-*N*-(6-methyl-2,4-bis-(methylthio)pyridin-3-yl)acetamide hydrochloride (**2**) (K-604), [28-31] an aqueous soluble ACAT-1 inhibitor developed from our lead compound 9-(benzo[*d*]oxazol-2-ylthio)-*N*-(2,6-diisopropylphenyl)nonanamide (**1**), [32] as shown in Figure 1.

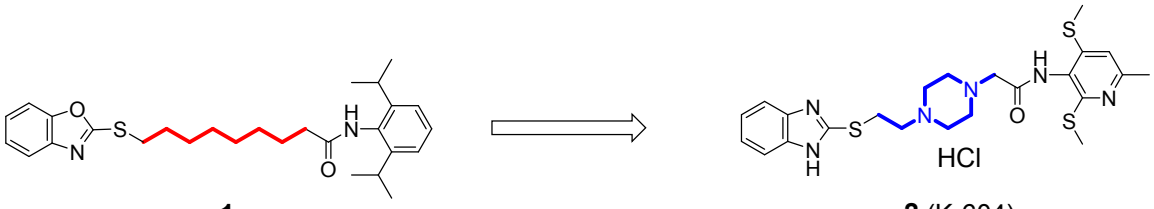

1

Rabbit aortic ACAT IC_{50} = 0.004 μM
Rabbit intestinal ACAT IC_{50} = 0.021 μM
cLogP 7.25
Aqueous solubility 0.03 μg/mL at pH 1.2

2 (K-604)

Rabbit aortic ACAT IC_{50} = 0.084 μM
Rabbit intestinal ACAT IC_{50} = 0.45 μM
Human ACAT-1 IC_{50} = 0.45 μM
Human ACAT-2 IC_{50} = 102.85 μM
LogP 3.3 at pH 6.8
Aqueous solubility 19 mg/mL at pH 1.2

Figure 1. Biological and physical properties of **2** (K-604), developed from our lead compound **1**

In a previous paper, [32] we reported our molecular design based on a double induced fit mechanism [33] for the feasible development of the aortic-selective ACAT inhibitor **1** and examined the pharmacological profile of this compound. Although **1** was efficacious when orally administered to high-fat- and cholesterol-fed F_1B hamsters, there remained room to considerably decrease the lipophilicity of this compound to increase aqueous solubility and consequently improve oral absorption and acceptable safety for further development of a clinical candidate. To address these issues, we used a solubility-driven structural optimization strategy; [34, 35] specifically, we focused on significant improvement of the physical properties via a small structural modification so that we could follow our established molecular design composed of two structurally different ligands (arylacetamide and benzazole) connected with a linker. We first focused on the structural accommodation of a linker moiety and the incorporation of basic amines into the molecule. In this paper, we report the molecular design strategy used to obtain an aqueous-soluble ACAT-1 inhibitor, **2** (K-604), as a clinical candidate, and we describe the structure-activity relationships (SARs), pharmacological properties, pharmacokinetic (PK) properties and safety test results of this compound.

Chemistry

To investigate the desired linker structure, the spatial arrangement and optimal bridging distance between the *N*-(2,6-diisopropylphenyl)acetamide unit (**A**) and the 2-(methylthio)benzo[*d*]oxazole unit (**B**) for maintenance of potency, and the intestinal IC_{50}/aortic IC_{50} selectivity ratio, we prepared the biological compounds for investigation as follows.

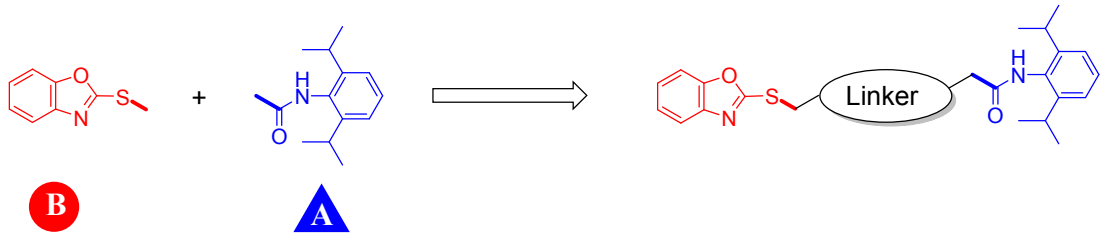

Figure 2. Exploration of the desired linker structure with a satisfactory spatial arrangement and an optimal distance between unit (**A**) and unit (**B**).

The synthetic routes used in this work are summarized in Schemes 1, 2, 3, 4, 5, 6 and 7.

Scheme 1. [a] Synthesis of compound **6,** which has a *trans*-olefin chain as a linker between the *N*-(2,6-diisopropylphenyl)acetamide unit (**A**) and 2-(methylthio)benzo[*d*]oxazole unit (**B**).

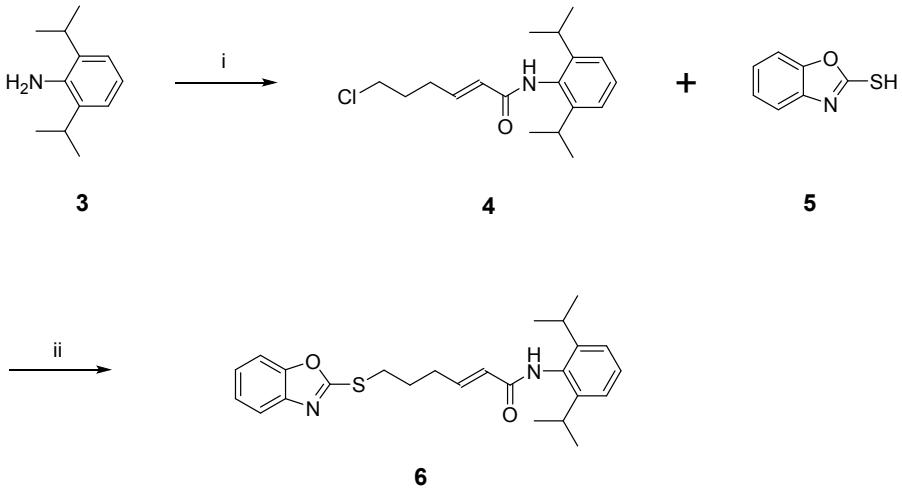

3 **4** **5** **6**

[a] Reagents and conditions: i) (*E*)-6-chloro-2-hexenoyl chloride, Et_3N, $CHCl_3$, rt, 46%; ii) 2-mercaptobenzo[*d*]oxazole (**5**), K_2CO_3, 18-crown-6, DMF, 80 °C then 100 °C, 30%.

(*E*)-6-Chloro-2-hexenoyl chloride was obtained as described in the literature [36] and subsequently used for acylation of 2,6-diisopropylaniline (**3**) to yield anilide **4**. The conversion to thioether **6** was achieved by reacting **4** with **5** in the presence of a base and a phase-transfer catalyst.

Scheme 2. [a] Synthesis of compound **9,** which has a benzene ring as a linker between the *N*-(2,6-diisopropylphenyl)acetamide unit (**A**) and 2-(methylthio)benzo[*d*]oxazole unit (**B**).

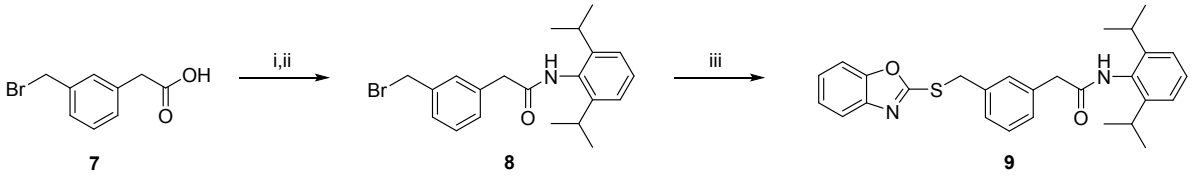

7 **8** **9**

[a] Reagents and conditions: i) $(COCl)_2$, cat. DMF, $CHCl_3$, rt; ii) **3**, Et_3N, $CHCl_3$, rt, 20% over 2 steps iii) **5**, K_2CO_3, 18-crown-6, DMF, 80 °C, 51%.

3-Bromomethylphenylacetic acid (**7**) was prepared from 2-(*m*-tolyl)acetic acid as described in the literature. [37] The acylation of **3** with **7** yielded anilide **8**, which was subsequently converted to thioether **9** as described in Scheme 1.

Scheme 3. [a] Synthesis of compound **22,** which has a *cis*-cyclohexane ring as a linker between the *N*-(2,6-diisopropylphenyl)acetamide unit (**A**) and 2-(methylthio)benzo[*d*]oxazole unit (**B**).

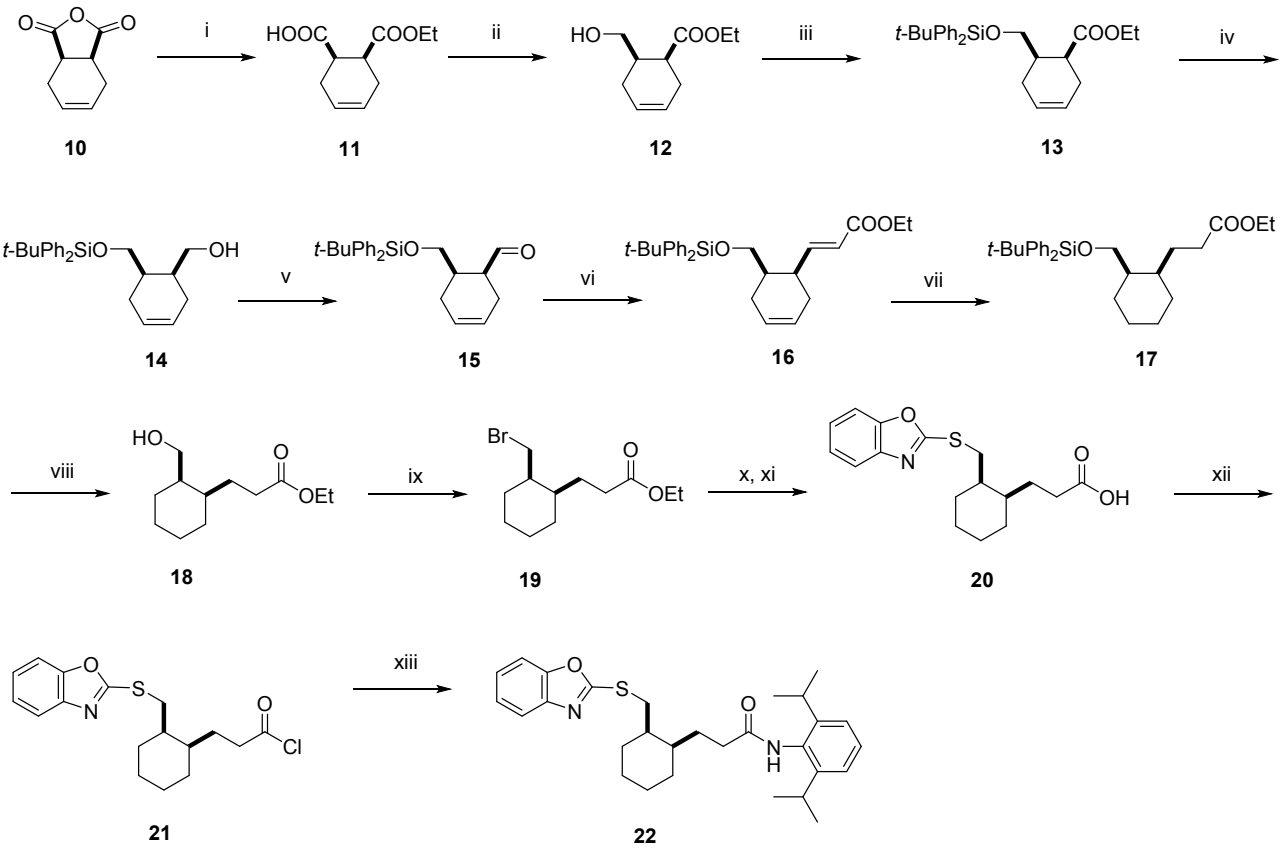

10 11 12 13 14 15 16 17 18 19 20 21 22

[a] Reagents and conditions: i) EtOH, reflux, 39%; ii) Et_3N, ClCOOEt, THF, 0 °C and then $NaBH_4$ /H_2O, THF, 0 °C, 51%; iii) *t*-Bu(Ph)$_2$SiCl, imidazole, DMF, rt, 73%; iv) DIBAL, toluene, -78 °C, 96%; v) Et_3N, $PySO_3$, DMSO, 0 °C; vi) NaH, $(EtO)_2P(O)CH_2COOEt$, THF, 0 °C then -78 °C, 89% over 2 steps; vii) H_2, Pd/C, EtOH, rt, 77%; viii) TBAF, THF, rt, 97%; ix) Ph_3P, NBS, CH_2Cl_2, rt, 78%; x) **5**, K_2CO_3, 18-crown-6, DMF, 80 °C, 89%; xi) 2 N NaOH, EtOH, 55 °C, 98%; xii) $(COCl)_2$, cat. DMF, $CHCl_3$, rt; xiii) **3**, Et_3N, $CHCl_3$, rt, 42% over 2 steps.

Solvolysis of *cis*-4-cyclohexene-1,2-dicarboxylic anhydride (**10**) in EtOH yielded the ring-opened ester **11**. Treatment of **11** with ethyl chloroformate and Et_3N in THF afforded the intermediate mixed anhydride, followed by reduction with $NaBH_4$ for conversion to alcohol **12**. Alcohol **12** was protected with *tert*-butyldiphenylchlorosilane in the presence of imidazole in

DMF to afford the TBDPS ether **13**. Reduction of **13** with DIBAL yielded alcohol **14**. Exposure of **14** to the sulfur trioxide-pyridine complex in DMSO yielded aldehyde **15,** which was treated with a phosphonate ylide prepared from NaH and triethyl phosphonoacetate to obtain acrylate **16**. Hydrogenation of **16** in the presence of Pd/C under a hydrogen atmosphere gave **17**, which was subjected to desilylation with TBAF to obtain alcohol **18**. Treatment of **18** with NBS and Ph_3P afforded bromo compound **19**. Reaction of **19** with **5** in the presence of K_2CO_3 and 18-crown-6 yielded a thioether, which was subsequently hydrolyzed by 2 N NaOH in EtOH to afford carboxylic acid **20**. Treatment of **20** with oxalyl chloride in the presence of a catalytic amount of DMF in $CHCl_3$ gave acid chloride **21**. The *N*-acylation reaction between **3** and **21** under basic conditions provided the desired anilide **22**.

Scheme 4. [a] Synthesis of compound **33,** which has a *trans*-cyclohexane ring as a linker between the *N*-(2,6-diisopropylphenyl)acetamide unit (**A**) and 2-(methylthio)benzo[*d*]oxazole unit (**B**).

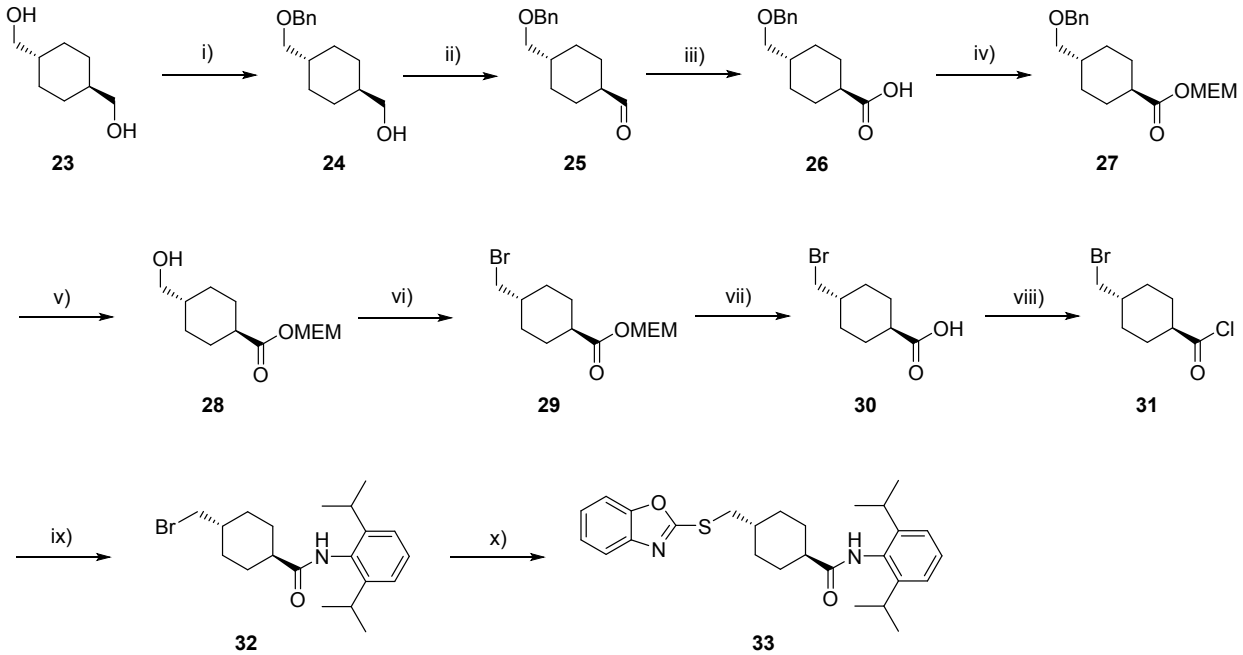

[a] Reagents and conditions: i) NaH, 15-crown-5, BnBr, DMF, 0 °C then rt, 45%; ii) Et_3N, $PySO_3$, DMSO, 0 °C; iii) Na_2HPO_4, 2-methyl-2-butene, $NaClO_2$, *t*-BuOH, H_2O, rt, 65% over 2 steps; iv) *i*-Pr_2EtN, MEMCl, CH_2Cl_2, 0 °C, 68%; v) H_2, Pd/C, EtOH, rt, 97%; vi) Ph_3P, NBS, CH_2Cl_2, rt, 43%; vii) 3 N HCl, THF, 40 °C, 85%; viii) $(COCl)_2$, cat. DMF, $CHCl_3$, rt; ix) **3**, Et_3N, $CHCl_3$, rt, 32% over 2 steps; x) **5**, K_2CO_3, 18-crown-6, DMF, 80 °C, 92%.

(*trans*-(4-(Benzyloxy)methyl)cyclohexyl)methanol (**24**) was prepared from *trans*-1,4-cyclohexanedimethanol (**23**) according to the method described in a patent application. [38] Exposure of **24** to the sulfur trioxide-pyridine complex in DMSO yielded aldehyde **25,** which was oxidized to carboxylic acid **26** by sodium chlorite. Protection of **26** with MEMCl in the presence of Hünig's base yielded MEM ester **27**. Hydrogenolysis of **27** in the presence of Pd/C under a hydrogen atmosphere yielded alcohol **28**. Treatment of **28** with NBS and Ph_3P afforded bromo compound **29**, which was deprotected under acidic condition to yield carboxylic acid **30**. Treatment of **30** with oxalyl chloride via a conventional procedure yielded acid chloride **31**. The *N*-acylation reaction between **3** and **31** under basic conditions yielded anilide **32**. The desired thioether **33** was obtained by the *S*-alkylation reaction of **5** with **32** under the conditions described above.

Scheme 5. [a] Synthesis of compound **38**, which has a 1,4-diazacycloheptane ring as a linker between the *N*-(2,6-diisopropylphenyl)acetamide unit (**A**) and 2-(methylthio)benzo[*d*]oxazole unit (**B**).

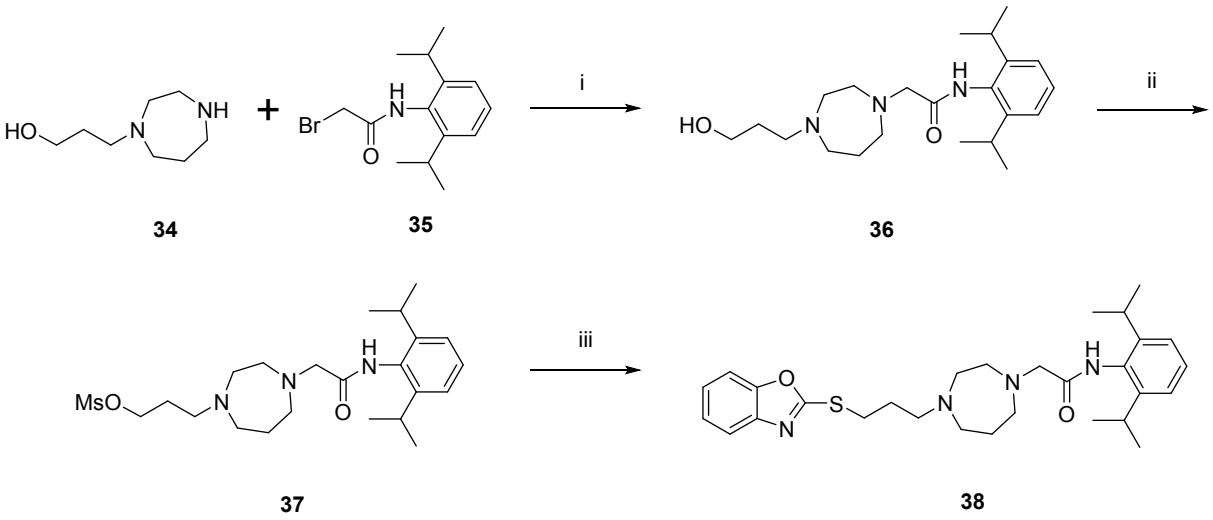

34 **35** **36** **37** **38**

[a] Reagents and conditions: i) K_2CO_3, MeCN, rt, 87%; ii) Et_3N, DMAP, MsCl, THF, 0 °C; iii) **5**, K_2CO_3, 18-crown-6, DMF, 80 °C, 81% over 2 steps.

The *N*-alkylation reaction between 3-(1,4-diazepan-1-yl)propan-1-ol (**34**) and 2-bromo-*N*-(2,6-diisopropylphenyl)acetamide (**35**) [32] provided anilide **36**, which was converted to mesylate **37** under the reaction conditions described above. The desired thioether **38** was obtained by reacting **37** with **5** in the conventional manner described above.

Scheme 6. [a] Synthesis of compound **42**, which has a 1,4-diazacyclohexane ring as a linker between the *N*-(2,6-diisopropylphenyl)acetamide unit (**A**) **a**nd 2-(methylthio)benzo[*d*]oxazole unit (**B**).

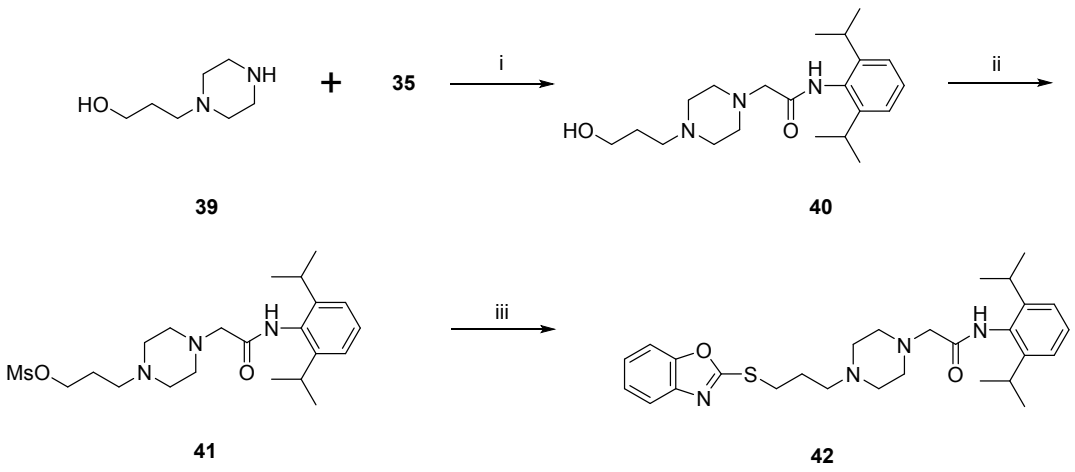

[a] Reagents and conditions: i) K_2CO_3, MeCN, 80 °C, 63%; ii) Et_3N, DMAP, MsCl, THF, 0 °C; iii) **5**, K_2CO_3, 18-crown-6, DMF, 80 °C, 60% over 2 steps.

The *N*-alkylation reaction between 3-(piperazin-1-yl)propan-1-ol (**39**) and **35** yielded the corresponding alcohol **40**, which was converted to mesylate **41** under the reaction conditions described above. The desired thioether **42** was obtained by reacting **41** with **5** under the reaction conditions described above.

Scheme 7. [a] Synthesis of compounds from **55** to **65**, with a 1,4-diazacyclohexane ring (lacking only one methylene unit) as a linker between a *N*-phenylacetamide or *N*-pyridylacetamide unit (**A**) and a 2-(methylthio)benz[*d*]azole or 2-(methylthio)oxazolo[*4,5-b*]pyridine unit (**B**).

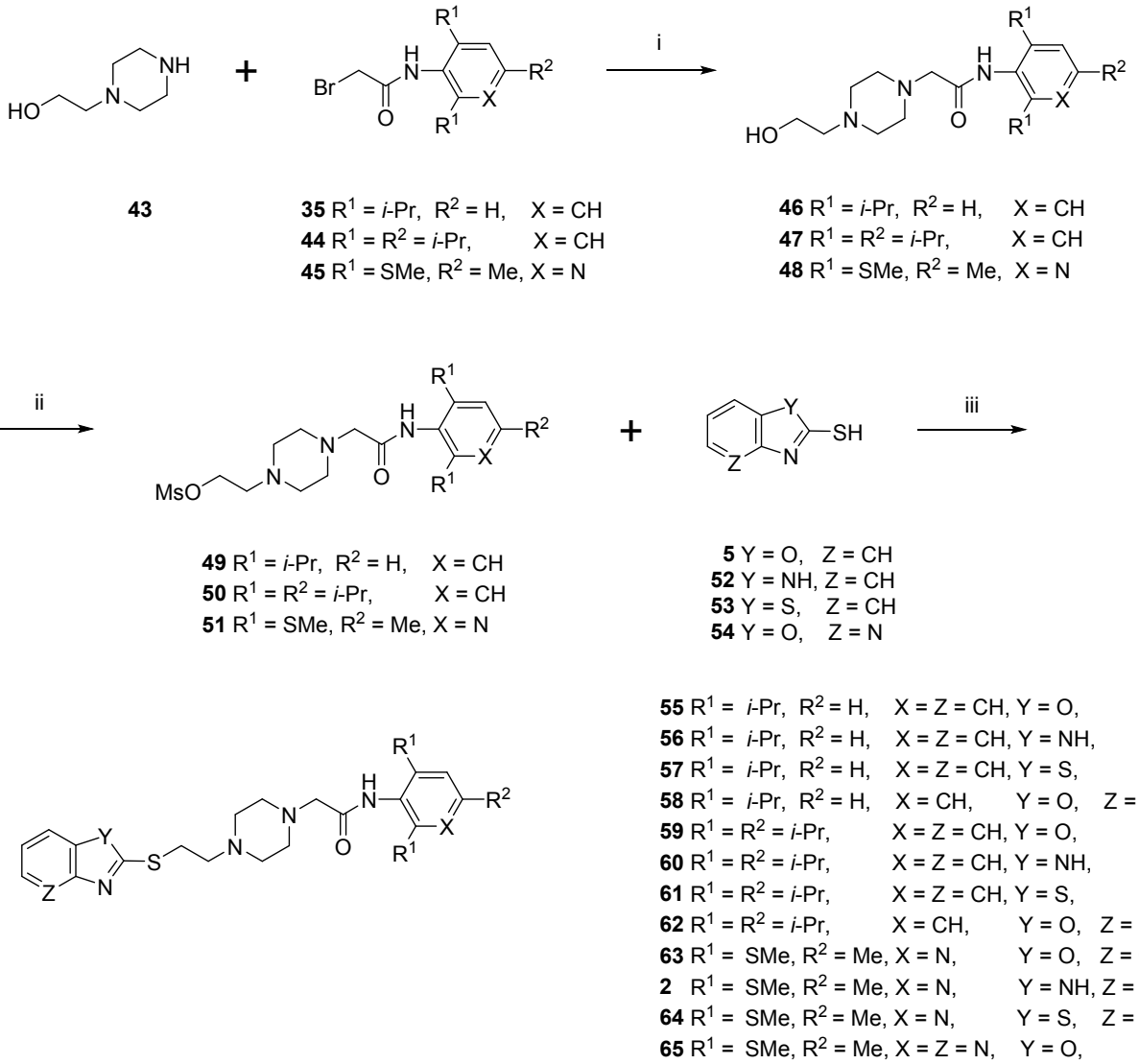

43

35 R^1 = *i*-Pr, R^2 = H, X = CH
44 R^1 = R^2 = *i*-Pr, X = CH
45 R^1 = SMe, R^2 = Me, X = N

46 R^1 = *i*-Pr, R^2 = H, X = CH
47 R^1 = R^2 = *i*-Pr, X = CH
48 R^1 = SMe, R^2 = Me, X = N

49 R^1 = *i*-Pr, R^2 = H, X = CH
50 R^1 = R^2 = *i*-Pr, X = CH
51 R^1 = SMe, R^2 = Me, X = N

5 Y = O, Z = CH
52 Y = NH, Z = CH
53 Y = S, Z = CH
54 Y = O, Z = N

55 R^1 = *i*-Pr, R^2 = H, X = Z = CH, Y = O,
56 R^1 = *i*-Pr, R^2 = H, X = Z = CH, Y = NH,
57 R^1 = *i*-Pr, R^2 = H, X = Z = CH, Y = S,
58 R^1 = *i*-Pr, R^2 = H, X = CH, Y = O, Z = N
59 R^1 = R^2 = *i*-Pr, X = Z = CH, Y = O,
60 R^1 = R^2 = *i*-Pr, X = Z = CH, Y = NH,
61 R^1 = R^2 = *i*-Pr, X = Z = CH, Y = S,
62 R^1 = R^2 = *i*-Pr, X = CH, Y = O, Z = N
63 R^1 = SMe, R^2 = Me, X = N, Y = O, Z = CH
2 R^1 = SMe, R^2 = Me, X = N, Y = NH, Z = CH
64 R^1 = SMe, R^2 = Me, X = N, Y = S, Z = CH
65 R^1 = SMe, R^2 = Me, X = Z = N, Y = O,

[a] Reagents and conditions: i) K_2CO_3, MeCN, 80 °C, 80−97% ; ii) Et_3N, DMAP, MsCl, THF, 0 °C; iii) **5**, **52**, **53** or **54**, K_2CO_3, 18-crown-6, DMF, 80 °C, 41−88% over 2 steps.

Similar to the reaction described above, the *N*-alkylation reaction between 3-(piperazin-1-yl)ethan-1-ol (**43**) and bromo compounds **35**, **44** and **45** yielded the corresponding alcohols **46**, **47** and **48**, which were converted to mesylates **49**, **50** and **51** under the reaction conditions described above. The desired thioethers from **55** to **65** were obtained by reacting mesylates **49**,

50 and **51** with 2-mercaptobenzo[*d*]oxazole (**5**), 2-mercaptobenz[*d*]-imidazole (**52**), 2-mercaptobenzo[*d*]thiazole (**53**) and 2-mercaptooxazolo[*4,5-b*]pyridine (**54**) under the reaction conditions described above.

Results and Discussion

The prepared compounds were evaluated for *in vitro* ACAT inhibition according to a modified version of the method described by Heider et al. [39] by using two enzyme sources: rabbit aorta homogenate and rabbit small intestine microsomes. The J774 macrophage cell culture assay was performed to assess the inhibition of the target cells by systemic antiatherosclerotic agents. [40] ACAT inhibition by all the prepared compounds is described herein and compared with that by our previously reported compound **1** [32] as an improvement index. The relationships between ACAT inhibition (IC_{50}) and the linker structure are summarized in Table 1. Based on compound **1** with the flexible linker, we investigated the impact of the intestinal IC_{50}/aortic IC_{50} selectivity ratio when the linker structure was slightly modified. Compound **6**, containing (*E*)-olefin, maintained almost a 5-fold selectivity whereas compound **9**, containing a benzene ring, lost selectivity. Interestingly, compound **33**, containing a spatially arranged *trans*-cyclohexane ring, exhibited a 9.6-fold increase in selectivity, whereas compound **22**, containing a *cis*-cyclohexane ring, was at 3.9-fold selective. It has been suggested that the spatially arranged *trans*-orientation in head-to-tail molecules might lead to low binding affinity with the intestinal ACAT and to weakening of intestinal ACAT inhibition, thereby enhancing the intestinal IC_{50}/aortic IC_{50} selectivity ratio.

Table 1. Effects of the spatial structure and arrangement of the linker between *N*-2,6-diisopropylaniline and 2-thiobenzo[*d*]oxazole on ACAT inhibition.

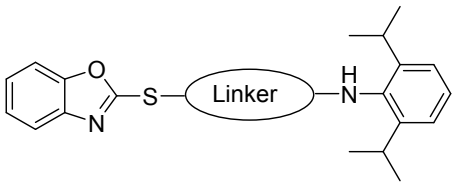

Compound	Linker Structure	Aortic IC_{50} (μM) [a]	Intestinal IC_{50} (μM) [b]	Intestinal/ Aortic Ratio	J774 Cells IC_{50} (μM) [c]	cLogP [d]
1	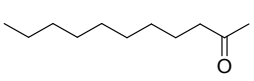	0.004	0.021	5.3	0.007	7.25
6	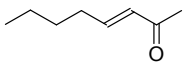	0.036	0.180	5.0	2.7	5.39
9	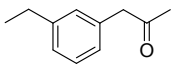	0.05	0.051	1.0	1.6	5.73
22	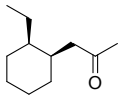	0.024	0.093	3.9	0.37	7.24
33	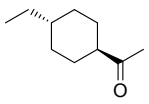	0.026	0.250	9.6	1.2	6.71
38	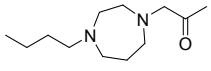	0.025	0.064	2.6	0.43	4.72
42	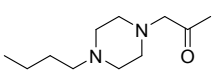	0.019	0.039	2.1	0.25	4.15

55	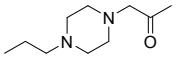	0.012	0.037	3.1	0.26	3.82

[a] IC_{50} (μM) against rabbit aortic ACAT activity. [b] IC_{50} (μM) against rabbit intestinal microsome ACAT activity. [c] IC_{50} (μM) against esterified cholesterol accumulation in J774 cells. [d] cLogP was calculated via ChemDraw/Pro 15.1.

Therefore, we envisioned the use of the spatial *trans*-orientation in our molecular design. Next, we focused on the role of the basic amine residue in order to improve aqueous solubility in acidic media, as shown in the following examples.

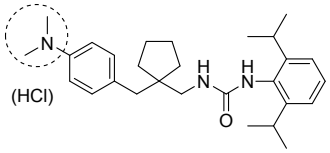

PD-132301
cLogP = 6.53
Solubility 2.18 mg/mL (pH 1.0)
PD-132301-2 (HCl)
Solubility 6.4 mg/mL (0.1-N HCl) lit. 41

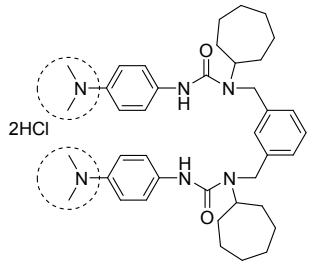

YM-17E
cLogP = 8.70
Solubility 10 mg/mL (0.025-N HCl) lit. 42

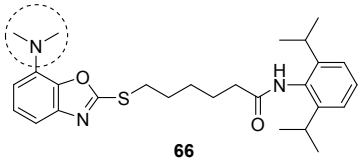

66
cLogP = 6.24
Solubility 0.18 mg/mL (pH 1.2)
IC_{50} = 0.036 μM (aorta)
IC_{50} = 0.077 μM (intestine)
IC_{50} = 0.820 μM (J774)

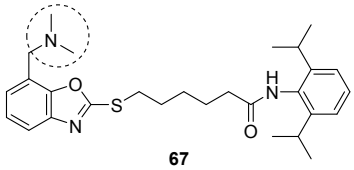

67
cLogP = 5.50
Solubility 0.4 mg/mL (pH 1.2)
IC_{50} = 0.096 μM (aorta)
IC_{50} = 0.130 μM (intestine)
IC_{50} = 5.60 μM (J774)

Figure 3. Physical and biological properties of ACAT inhibitors containing a *N,N*-dimethylamino group and a *N,N*-dimethylaminomethyl group

As shown in Figure 3, introduction of the *N,N*-dimethylamino group into molecules such as 1-(2,6-diisopropylphenyl)-3-((1-(4-(dimethylamino)benzyl)cyclopentyl)methyl)urea (PD-132301) [41] and 1,1'-(1,3-phenylenebis(methylene))bis(1-cycloheptyl-3-(4-(dimethylamino)phenyl)urea) dihydrochloride (YM-17E) [42] has been very effective at increasing aqueous solubility in acidic media. Comparison of compounds **66** and **67** [32] shows that the *N,N*-dimethylaminomethyl group also contribute to doubling the aqueous solubility (from 0.18 to 0.4 mg/mL) by increasing the basicity but dramatically decreased ACAT inhibition in J774 cells. As reported previously, [32] the polar-ionic interaction around the binding site not only negatively affected the adaptability of the ligand-binding pocket or cleft in our head-to-tail design but also potentially obstructed the molecular permeability of the J774 cell membrane. Accordingly, this insight led us to incorporate two nitrogen atoms into the linker. Compound **38** (with a homopiperazine linker) had a ca. 2 orders of magnitude lower cLogP value than that of **33** (with a *trans*-cyclohexane linker) but successfully maintained the inhibitory activity toward aortic ACAT. Notably, **42** and **55** (with piperazine linkers lacking one or two methylene units) exhibited slightly more potent inhibitory activity toward intestinal ACAT and J774 cells than **38**. Having succeeded in minimizing the value of cLogP from 4.72 to 3.82, we next investigated the appropriate combination of substituent groups ($R^1 = R^2$ and/or R^3) and atoms (X, Y, Z) based on the template structure of **55**. The ACAT inhibitory activities of compounds **55** to **65** are summarized in Table 2.

Table 2. Effects of the substituent groups and incorporated hetero atoms at each position on the 1,3-benzazole moiety (Y = O, NH, or S; Z = CH or N) and arylacetamide moiety (X = CH or N and substituent groups $R^1$and R^2) on ACAT inhibition.

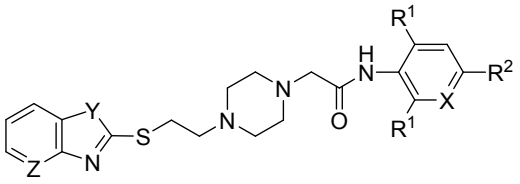

Compound	R^1	R^2	X	Y	Z	Aortic IC_{50} (μM) [a]	Intestinal IC_{50} (μM) [b]	Intestinal/ Aortic Ratio	J774 Cells IC_{50} (μM) [c]	cLogP [d]
55	*i*-Pr	H	CH	O	CH	0.012	0.037	3.1	0.26	3.82
56	*i*-Pr	H	CH	NH	CH	0.11	0.51	4.6	0.28	3.97
57	*i*-Pr	H	CH	S	CH	0.016	0.036	2.3	0.17	4.49
58	*i*-Pr	H	CH	O	N	0.11	0.32	2.9	0.45	2.77
59	*i*-Pr	*i*-Pr	CH	O	CH	0.034	0.270	7.9	0.25	5.24
60	*i*-Pr	*i*-Pr	CH	NH	CH	0.23	0.41	1.8	0.49	5.39
61	*i*-Pr	*i*-Pr	CH	S	CH	0.13	0.31	2.4	0.41	5.92
62	*i*-Pr	*i*-Pr	CH	O	N	0.30	1.3	4.3	0.37	4.19
63	SMe	Me	N	O	CH	0.033	0.029	0.9	0.009	4.07
2	SMe	Me	N	NH	CH	0.084	0.45	5.4	0.026	4.22
64	SMe	Me	N	S	CH	0.041	0.038	0.9	0.003	4.78
65	SMe	Me	N	O	N	0.12	0.21	1.8	0.1	3.02

[a] IC_{50} (μM) against rabbit aortic ACAT activity. [b] IC_{50} (μM) against rabbit intestinal microsome ACAT activity. [c] IC_{50} (μM) against esterified cholesterol accumulation in J774 cells. [d] cLogP was calculated by ChemDraw/Pro 15.1.

For selection of precandidate aqueous-soluble ACAT inhibitors, we set the threshold value for ACAT inhibitory activity (μM) against J774 cells as 0.1 and that for cLogP as 4.3, which were low and reasonably achievable. Finally, we selected **2**, **63** and **65** and evaluated the lipid-modulating abilities (CE /free cholesterol (FC) ratio) of these compounds in each organ, which

would be ultimately the same output as that for the treatment of incurable diseases that involve ACAT-1 overexpression. The evaluation was performed with a diet-induced atherosclerosis model using Bio F_1B hamsters as described previously. [32] To investigate potential drug exposure, we conducted a PK study using precandidates **2**, **63** and **65**, which were orally administered to nonfasted male rats at a dose of 30 mg/kg.

Table 3. Comparison of the physical and PK properties [a] of precandidates **2**, **63** and **65** with those of the lead compound **1** under nonfasted conditions [b].

Compound	**1** [c]	**2**	**63**	**65**
Solubility at pH 1.2	0.03 μg/mL	19 mg/mL	17 mg/mL	33 mg/mL
Tmax	3.2 h	0.7 h	2.8 h	0.5 h
Cmax	107 ng/mL	192 ng/mL	158 ng/mL	1038 ng/mL
$T_{1/2}$	ND [d]	2.1 h	10.1 h	3.4 h
AUC_{inf}	358 ng·h/mL	594 ng·h/mL	4125 ng·h/mL	2825 ng·h/mL

[a] The values are the means of > 3 experiments ± standard deviations (SDs). [b] A 30 mg/kg dose (**1**) in 0.5% MC suspension solution and (**2**, **63** and **65**) in 0.05 N HCl solution were orally administered to male rats (n = 3) under nonfasted conditions. [c] The data shown for compound **1** was cited from our previous paper.[32] [d] ND (not determined) because the drug concentration for one rat continued to increase 6 h after administration, while that for the other two rats remained stable.

As shown in Table 3, the compounds with the piperazine linker, namely, **2**, **63** and **65**, exhibited dramatically enhanced aqueous solubilities, with values of 19, 17 and 33 mg/mL, respectively. These major improvements led to an 11.5- and 7.9-fold increase in the drug exposure (AUC_{inf}) of **63** and **65**, respectively, compared with that of **1**. To determine the doses of the three compounds,

we considered the weakest activity (0.1 μM) of **65** against J774 macrophages and determined the doses of **2** and **63** (1, 3, 10 and 30 mg/kg) and those of **65** (3, 10, 30 and 100 mg/kg) for the dietary drug administration study, which utilized Bio F_1B hamsters fed a diet that was high in fat and cholesterol for 10 weeks.

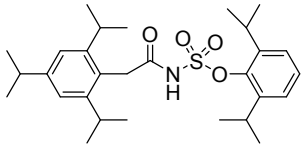

CI-1011

IC_{50} = 31 μM (rabbit aorta homogenate) [32]
IC_{50} = 13 μM (rabbit intestinal microsomes)

In the cholesterol-fed F_1B hamster model [43]
Reduction of lipid accumulation area with decreasing plasma TC
68% at a dose of 3 mg/kg
86% at a dose of 10 mg/kg
93% at a dose of 30 mg/kg

Figure 4. Structure and pharmacological properties of **CI-1011**

2,6-Diisopropylphenyl(2-(2,4,6-triisopropylphenyl)acetyl)sulfamate (CI-1011, Avasimibe) [43-49] demonstrated hypolipidemic and antiatherosclerotic effects in several animal models and was in phase III clinical trials. We used this compound as reference compound for *in vivo* tests.

The nonselective ACAT inhibitor **63** at doses of 3, 10 and 30 mg/kg significantly decreased the lipid accumulation areas in the aortic arch (37, 32 and 28% relative to the control, respectively) along with reducing the total cholesterol (TC) level in the plasma (73, 28 and 24% relative to the control, respectively). The pharmacological behavior of **63** was similar to that of **CI-1011**. Interestingly, the weakest ACAT inhibitor, **65**, even at doses of 3 and 10 mg/kg, markedly decreased the lipid accumulation areas (49 and 34% relative to the control, respectively) without decreasing the plasma TC level, as shown in Figure 5. The potent inhibitor **2,** with a higher selectivity toward aortic ACAT than **65**, showed only moderate effects on the lipid accumulation areas (71 and 53% relative to the control, respectively) at the same doses. Next, we asked why **65** had a strong effect on the aortic ACAT. The PK profile indicated that **65** had a high Cmax (1038

ng/mL), a short Tmax (0.5 h) and a rather large AUC_{inf} (2825 ng·h/mL) with a $T_{1/2}$ of 3.4 h, while **2** exhibited a low Cmax (192 ng/mL) and a short Tmax (0.7 h) but a moderate AUC_{inf} (594 ng·h/mL) with a short $T_{1/2}$ (2.1 h). Based on the ACAT inhibitory activities of both compounds (**2**: IC_{50} = 0.026 μM *vs* **65**: IC_{50} = 0.1 μM) toward J774 cell macrophages (i.e., antifoaming action), the effective capacity (F) of ACAT inhibitors could be expressed as an index by the following equation: F = Cmax/MW/IC_{50}. The F value of **2** was calculated to be 14.7, whereas that of **65** was 20.6. Accordingly, the effective capacity of **2** was ca. 70% as much as that of **65**. The actual lipid accumulation areas of **65** at doses of 3 and 10 mg/kg (49 and 34% relative to the control, respectively) were consistent with the calculated areas for **2** (71 × 0.7 = 50 and 53 × 0.7 = 37% relative to the control, respectively).

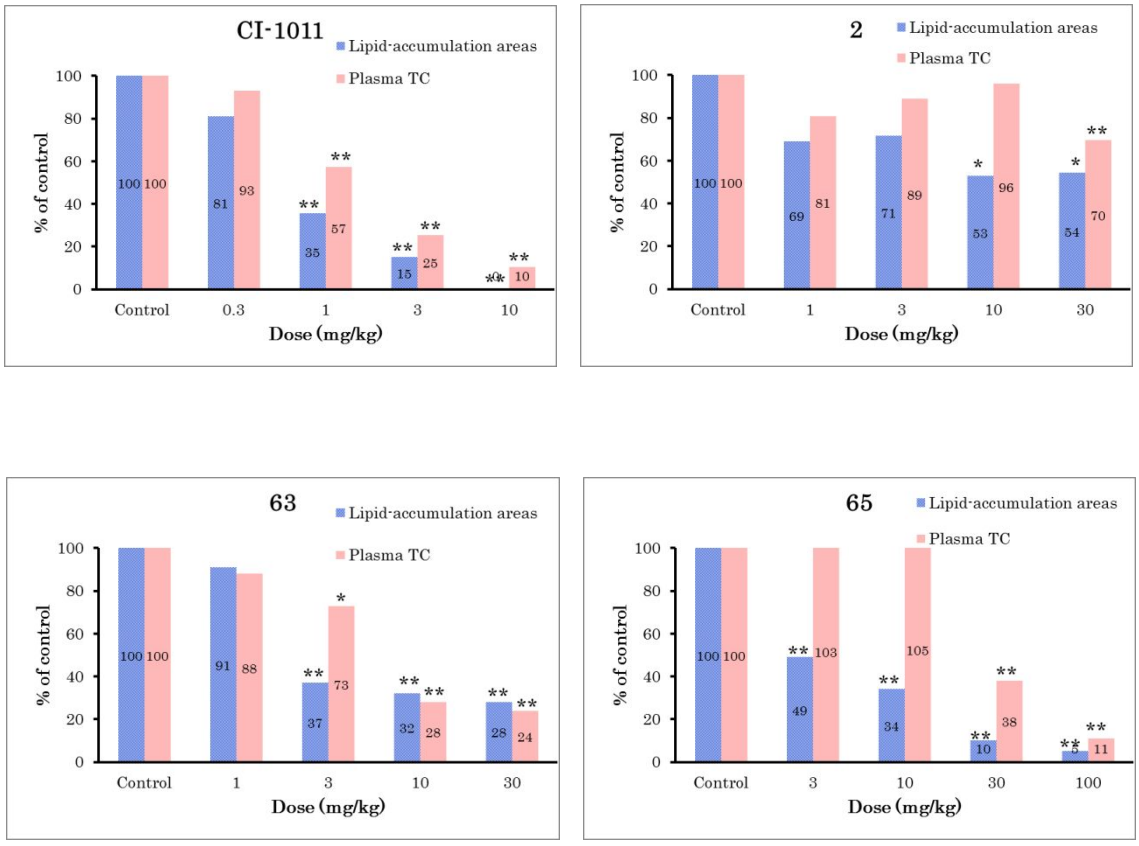

Figure 5. Effects of **CI-1011**, **2**, **63** and **65** on the plasma TC levels and lipid accumulation areas.

Compounds **2** and **63** were administered at doses of 1, 3, 10, 30 mg/kg, whereas **65** was administered at doses of 3, 10, 30, 100 mg/kg, via the diet to Bio F_1B hamsters fed a diet that was high in fat and cholesterol. The control compound **CI-1011** was used at the same dose setting (0.1, 1, 3, 10 mg/kg) that was described previously. [32] The % value ± SD was calculated relative to the control. * $p<0.05$ and ** $p<0.01$ vs. control; statistical analysis was conducted using Dunnett's test.

As shown, the F value allowed estimation of both pharmacological effects. On the other hand, the nonselective ACAT inhibitor **63** exhibited a low Cmax (158 ng/mL) with a medium Tmax (2.8 h), but exhibited the largest AUC_{inf} (4125 ng·h/mL) with a long $T_{1/2}$ (10.1 h). This compound acted on the liver and intestinal ACAT over a long duration and contributed a significant decrease in the plasma TC levels for the suppression of lipid accumulation areas. Therefore, the pharmacodynamics (PD) of aortic ACAT might be more significantly affected by a large Cmax than by a large AUC_{inf}. In fact, a transient exposure of aortic ACAT to a large amount of drug might prolong the duration of the inhibitory effect on aortic ACAT. In other words, the inhibition of aortic ACAT seems to be different from that of other enzymes, such as HMG-CoA reductase. [50-53] To further elucidate the lipid-modulating potential of **2**, **63** and **65** in each organ, we measured the CE/FC ratio in the plasma, liver, intestine and adrenal gland. The relative relationships of the ratio of the change in lipid accumulation areas and plasma TC levels and the lipid proportion ratio (CE/FC) in the liver, intestine and adrenal gland with the dose responses are presented as scatter plot graphs in Figure 6.

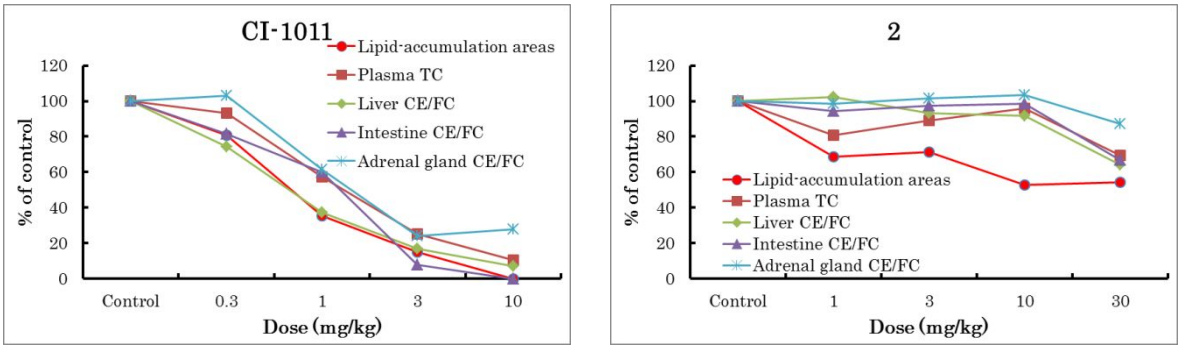

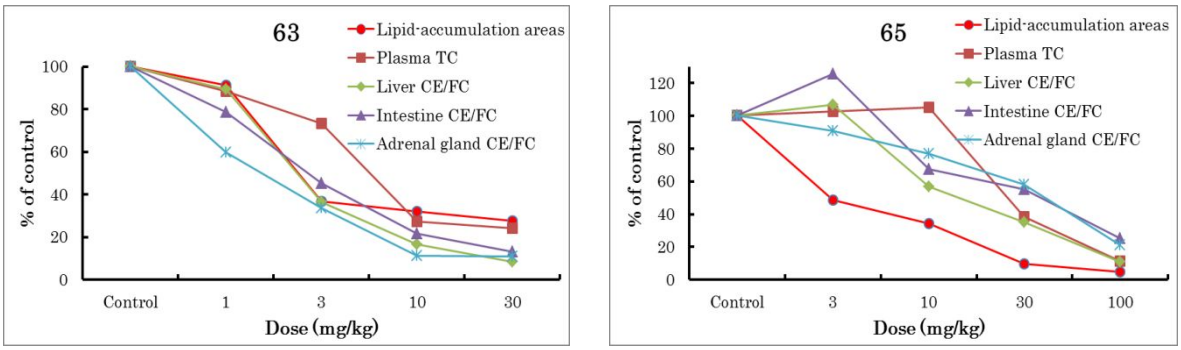

Figure 6. Relationships of the relative ratios of lipid accumulation areas and plasma TC levels and the lipid proportion ratio (CE/FC) in the liver, intestine and adrenal gland with the dose responses.

In the scatter plot graphs, the pharmacological profile of the ACAT inhibitors precisely indicated the degree of the effect on each organ. As nonselective ACAT inhibitors, the slopes of all the lines for **63** were similar to those for **CI-1011**. In contrast, both inhibitors **2** and **65** exhibited large discrepancies between the plasma TC lines and the lipid accumulation area lines, which were positioned the lowest. This important finding reveals aortic-selective ACAT inhibition *in vivo*. Notably, the adrenal gland CE/FC lines for **CI-1011**, **2** and **65** were positioned the highest, whereas that for **63** was the lowest. **CI-1011** has actually been reported to have a low adrenal effect. [54] This behavior was consistent with the results of our preliminary adrenal toxicity test after 24 h when single intravenous injection of **63** or **65** were administered to male rabbits. This test had the advantage of predicting adrenal toxicity in a sensitive and prompt manner, [55] in contrast to the toxicity test that involved repeated oral administration over a long period. While **63** induced the necrosis of adrenal zona fasciculata cells in three of four rabbits, even at a dose of 0.1 mg/kg, **65** exhibited similar toxicity in one of four rabbits at a dose of 5 mg/kg. The toxicity level of **63** was revealed to be the same as that of **PD-132301-2**, which was a positive control. [56-59] The no-observed-adverse-effect level (NOAEL) of **CI-1011** was determined to be 5 mg/kg.

Accordingly, the adrenal gland CE/FC line can be regarded as a safety index for adrenal toxicity. At this stage, **65** was the most attractive aortic-selective ACAT inhibitor with good exposure and safety. For further profiling of **2**, **63** and **65** before selection of a clinical candidate, we assessed the compounds via the full Ames test (TA98, TA100, TA1535, TA1537, WP*uvrA*) and the chromosomal aberration test. Although the three precandidates passed the Ames test, the compounds **63** and **65** tested positive in the chromosomal aberration test (Supporting Information). In the three compounds **2**, **63** and **65**, *N*-(6-methyl-2,4-bis(methylthio)pyridin-3-yl)acetamide was a common structure in the head moiety. We concluded that the potential genotoxicity originated from the structure of the 2-thiobenzo[*d*]oxazole and 2-thiooxazolo[*4,5-b*]pyridine group in the tail moiety. Unexpectedly, both compounds **63** and **65** were identified as unstable substrates upon exposure to acidic medium in the chemical stability test (Supporting Information). Therefore, we abandoned the development of **63** and **65** as active pharmaceutical ingredients (APIs). Next, we focused our efforts on further pharmacological studies of **2**. As previously reported, we verified the isoform selectivity of **2** using human ACAT-1 and ACAT-2 and identified this compound to be a potent ACAT-1 inhibitor with 229-fold selectivity for ACAT-2. [30] Having investigated the reason underlying the large discrepancy in the value of isoform selectivity between human ACATs and rabbit ACATs in an ACAT assay system, we recently reported that the binding of the plasma protein with the substrate is crucial for the measurement of ACAT inhibition in the conventional assay. According to the reported simulation, [32] the aortic IC_{50} value (84 nM) of **2** decreased to 2.3 nM when using the rabbit unbound plasma fraction (fp) (2.7%) (Supporting Information). Due to plasma protein binding, the IC_{50} of aortic ACAT inhibition was weakened from approximately 2.3 nM to 84 nM. On the other hand, the intestinal ACAT inhibition (450 nM) in the digestive tract was not affected;

therefore, the value of isoform selectivity was identified to be approximately 196 (450 divided by 2.3 is 195.6). [60] This simulation result is consistent with human ACAT isoform selectivity and accounts for the obtained pharmacological behavior *in vivo*. In the precise evaluation of F_1B hamsters on a high-fat diet, the suppression of lipid accumulation areas could be significantly compensated even at a dose of ≥1 mg/kg **2** without affecting the plasma TC levels when dietary administration was replaced with oral administration. [30] We interpreted that the reduction in dosing was attributed to a ca. 3-fold increase in drug exposure by switching to oral drug administration from dietary administration; the data showed that the Cmax was 568 ng/mL when the drug was orally administered to fasted male rats at a dose of 30 mg/kg. Furthermore, when apoE-knockout mice were treated for 12 weeks with a dose of 60 mg/kg, we observed the direct plaque-modulating effects of **2** on the vascular wall independently of the plasma TC levels. [31] In the event of acute coronary syndrome (ACS), vulnerable plaques are characterized by accumulation of macrophage-derived foam cells and thin fibrous caps, while stable plaques are characterized by collagen-rich fibrous caps with fewer macrophages than vulnerable plaques. Rupture of the fibrous cap may occur, thereby exposing highly procoagulant material to the circulating blood, leading to occlusive thrombus formation and subsequent ischemia or infarction. [61] Therefore, our final therapeutic goal is to transform vulnerable plaque into stable plaque for the prevention of plaque rupture. Having observed a potentially therapeutic effect in the prevention of ACS, we next conducted a PK study of **2** when orally administered to fasted and nonfasted dogs for extrapolation of human PK.

Table 4. Comparison of the pharmacokinetic properties [a] of **2** under fasting and nonfasting conditions [b].

Condition	Tmax (h)	Cmax (ng/mL)	Area under the curve (AUC) 0-8 h (ng· h/mL)
Nonfasted	2.3 ± 1.3	1424 ± 1649	3575 ± 4012
Fasted	1.0 ± 0.7	5466 ± 4010	13932 ± 7825

[a] Data are shown as the means ± SDs. [b] A 10 mg/kg dose in capsules was orally administered to male dogs (n = 4) under fasting and nonfasting conditions.

As shown in Table 4, interestingly, the Cmax and AUC_{inf} values for the aqueous-soluble compound **2** under fasting conditions were 3.8-fold higher than those under nonfasting conditions. This finding is a positive sign in terms of safety test. Because the NOAEL of the highly lipophilic compound **1** could not be determined, saturation of drug exposure was reached due to poor absorption in male dogs at doses of 30 and 100 mg/kg over 2 weeks. The improvement of drug exposure between lead compound **1** and candidate compound **2** is summarized in Figure 7. The marked enhancement of aqueous solubility (up to 19 mg/mL at pH 1.2) led to dramatic improvement of oral absorption (the Cmax of **2** was 1100-fold higher than that of **1** in fasted dogs).

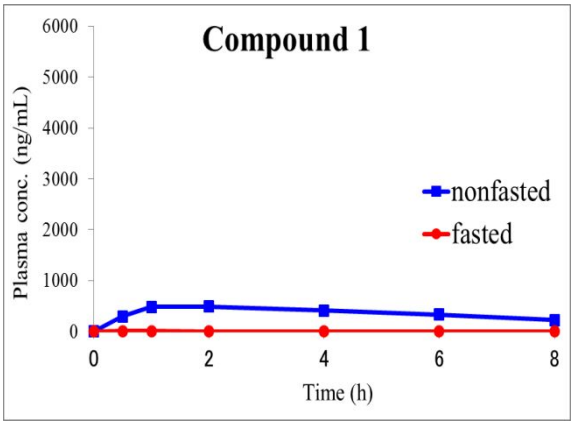

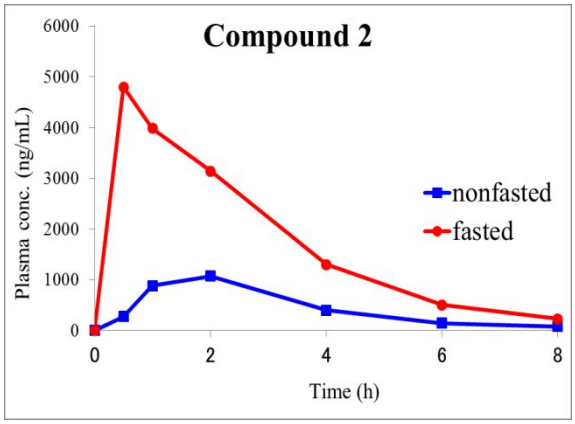

Figure 7. Plasma drug concentration of **1** at a dose of 30 mg/kg [a] and **2** at a dose of 10 mg/kg after a single oral administration to male dogs (n = 3 and n = 4) under nonfasting or fasting conditions. [a] The data for compound **1** was cited from our previous paper. [32]

In safety tests for **2**, the NOAELs were determined to be 10 mg/kg in both dogs (4 weeks) and monkeys (26 weeks) without sex discrimination. At the beginning of this study, we were very concerned about whether the adrenal toxicity could be avoided. To investigate this issue, the drug tolerance of a healthy volunteer in a phase 1 study far surpassed the safety threshold (Cmax, 1 μg/mL, AUC, 3 μg·h/mL) observed in the safety test for monkeys. In a phase II study, the clinical candidate **2** showed stable linear exposure in terms of Cmax and AUC between the low- and high-dose groups for 26 weeks. In a clinical study on the prevention and early intervention of cardiovascular disease, the lipid profiles of patients should be well controlled to decrease plasma TC levels to 171 mg/dL and low-density lipoprotein cholesterol (LDL-C) levels to 101 mg/dL by statin. [8] We stated that a so-called add-on therapy with statin would hinder the assessment of the capability of ACAT inhibitors. Based on our experience, [62] we wondered whether it would be appropriate to evaluate the efficacy of ACAT inhibitors under circumstances where ACAT activity would be markedly downregulated. We believe that it would be beneficial for research to be focused on diseases that involve ACAT-1 overexpression, such as aggressive cancers and Alzheimer's disease, which is independent of cholesterol metabolism in the brain.

Conclusion

Starting from the highly lipophilic aortic ACAT inhibitor **1**, we used a solubility-driven structural optimization and inserted a piperazine unit in the place of a 6-methylene chain into the

linker region. By optimization and selection, we have overcome several drawbacks associated with **1** and succeeded in obtaining the marked improvement of the aqueous solubility (up to 19 mg/mL at pH 1.2) and oral absorption (the Cmax of **2** was 1100-fold higher than that of **1** in fasted dogs) of **2** compared with those of **1**. We also serendipitously discovered **2** to be a potent inhibitor of human ACAT-1, with 229-fold selectivity for this protein over human ACAT-2, and demonstrated the unique pharmacological effects of this compound in plaque stabilization. After this compound passed safety tests, we designated **2** as a clinical candidate named **K-604**, which was found to be well tolerated in a phase 1 study and maintained stable exposure over 26 weeks in a phase 2 clinical study. Rather than the treatment of atherosclerosis, we believe that **K-604** has potential therapeutic applications for the treatment of incurable diseases that involve ACAT-1 overexpression. Recently, we succeeded in establishing an intranasal administration method for efficient delivery of **K-604** into the brain, which made it possible to substantially modulate brain cholesterol levels in a smooth manner despite a short duration of exposure. We will report these results in the near future.

Experimental Section

All procedures performed on animals in this study were in accordance with established guidelines and regulations and were reviewed and approved by the Committee on the Ethics of Animal Experiments, Kowa Company Ltd.

We computationally checked all active compounds for PAINS and found that they were negative.

Chemistry.

Commercially available reagents and solvents were used without further purification. Thin-layer chromatography (TLC) analyses were conducted using silica gel 60 F254 plates (Merck). ^{1}H-nuclear magnetic resonance (NMR) spectra were recorded using a JEOL JNM-LA 400 MHz and JEOL GSX-270. Tetramethylsilane was used as an internal standard for spectra obtained in deuterated dimethyl sulfoxide (DMSO-d_6) and $CDCl_3$. Chemical shifts (δ) are given in parts per million (ppm), and coupling constants (J values) are given in hertz (Hz) and reported to the nearest 0.1 Hz. Infrared (IR) spectra were recorded using a JASCO ALOR-III. Mass spectra were obtained on a JEOL MS-BU20 mass spectrometer (MS). Low-resolution mass spectra were recorded on a JEOL JMS-D-300 MS. Elemental analyses (C, H, and N) were performed using Yanaco MT-5. Melting points were determined in open glass capillaries using a Buchi B-545 melting point apparatus. Purities of all test compounds were greater than 95% based on HPLC chromatogram on a Shimadzu LC-20A series. LC/MS system (Shimadzu LC-10A and AB Sciex API 165) were used for the measurement of plasma drug concentration.

Materials

3-(1,4-Diazepan-1-yl)propan-1-ol, 3-(piperazin-1-yl)propan-1-ol and 2-mercaptooxazolo[4,5-b]pyridine were commercially available.

The syntheses of the target compounds **2**, **63**, and **65** are described below. Detailed experimental procedures for the syntheses of all other compounds, their intermediates and the characterization data are provided in the Supporting Information.

Representative synthetic procedure for compounds 2, **63** and **65**.

2-[4-[2-(Benzimidazole-2-ylthio)ethyl]piperazin-1-yl]-*N*-(2,4-bis(methylthio)-6-methyl-3-pyridyl)acetamide (the free amine of 2). 6-Methyl-2,4-bis(methylthio)pyridin-3-amine was obtained according to a method described in a patent (WO9104027, Sep 15, 1989). Step 1. A solution of bromo acetylbromide (62.7 g, 0.311 mol) in CH_2Cl_2 (200 mL) was added dropwise to a stirred solution of 6-methyl-2,4-bis(methylthio)pyridin-3-amine (60.1 g, 0.30 mol) and *N,N,*-dimethylaniline (47.9 g, 0.395 mol) in CH_2Cl_2 (300 mL) at 0 °C over 1 h. The reaction mixture was allowed to stand at 0 °C for 12 h. The precipitated salt was filtered out and washed with cold EtOH (300 mL) and Et_2O (300 mL) to yield 2-bromo-*N*-(6-methyl-2,4-bis(methylthio)-pyridin-3-yl)acetamide (**45**) (64.2 g, 67%) as colorless fine needles. The combined filtrates (mother liquors) were concentrated under reduced pressure. The residue was dissolved in $CHCl_3$ (100 mL) and crystalized from Et_2O (200 mL) to yield **45** (12.37 g, 13 %) as colorless powdery crystals. Mp 157-158 ℃; IR (KBr) cm^{-1}: 3222, 3184, 3042, 2999, 1668, 1565, 1522; ^{1}H-NMR ($CDCl_3$) δ: 2.43 (3H, s), 2.50 (3H, s), 2.53 (3H, s), 4.07 (2H, s), 6.67 (1H, s), 7.58 (1H, br s); Anal. Calcd for $C_{10}H_{13}BrN_2OS_2$: C, 37.39; H, 4.08; N, 8.72; Br, 24.87; S, 19.96. Found: C, 37.41; H, 4.08; N, 8.59; Br, 24.99; S, 20.13. Step 2. K_2CO_3 (37.5 g, 0.271 mol) was added to a solution of 1-(2-hydroxyethyl)piperazine (**43)** (35.3 g, 0.271 mol) and **45** (64.2 g, 0.20 mol) in MeCN (1.2 L) under ice-cold conditions. The reaction mixture was allowed to warm to rt, stirred for 23 h, and then diluted with water (1.0 L) and $CHCl_3$ (1.5 L). The organic layer was removed. The aqueous layer was extracted with $CHCl_3$ (0.5 L × 2). The combined organic layers were washed with brine, and dried over $MgSO_4$. After filtration, the solvent was evaporated *in vacuo*. The residue was recrystallized from EtOH/Et_2O to afford 2-(4-(2-hydroxyethyl)piperazin-1-yl)-*N*-(6-methyl-2,4-bis(methylthio)pyridin-3-yl)acetamide (**48**) (71.9 g, 97%) as colorless crystals. Mp 119-120℃; IR (KBr) cm^{-1}: 3336, 1687, 1564, 1534, 1478 ; ^{1}H-NMR ($CDCl_3$) δ:

2.42 (3H, s), 2.50 (3H, s), 2.52 (3H, s), 2.66 (2H, t, J = 5.4 Hz), 2.67-2.90 (8H, m), 3.23 (2H, s), 3.69 (2H, t, J = 5.4 Hz), 6.67 (1H, s), 8.49 (1H, br s); Anal. Calcd for $C_{16}H_{26}N_4O_2S_2$: C, 51.86; H, 7.07; N, 15.12; S, 17.31. Found: C, 51.84; H, 7.00; N, 14.92; S, 17.34. Step 4. Et_3N (48.5 g, 0.479 mol) and DMAP (1.76 g, 14.4 mmol) were added to a solution of **48** (105 g, 0.286 mol) in THF (1.4 L), followed by dropwise addition of MsCl (42.0 g, 0.366 mol) at 0 °C. The reaction mixture was stirred at the same temperature for 1 h. After filtration, the precipitated salt was removed, and the filtrate was concentrated *in vacuo*. Step 5. The residue was dissolved in DMF (1.0 L). Compound **52** (48.6 g, 0.323 mol), K_2CO_3 (48.58 g, 0.351 mol) and 18-crown-6 (3.56 g, 13.5 mmol) were added to this solution at rt. The reaction mixture was stirred at 80 °C for 3 h and concentrated *in vacuo*. The residue was dissolved in $CHCl_3$ (2.0 L) and diluted with water (2.0 L). The aqueous layer was extracted with $CHCl_3$ (1.0 L × 2). The combined organic layers were washed with brine, and dried over $MgSO_4$. After filtration, the solvent was evaporated *in vacuo*. The residue was purified by silica gel column chromatography, and eluted with *n*-hexane/acetone (3:1) to afford an oil, which was further purified by silica gel column chromatography, and eluted with MeOH/$CHCl_3$ (1:100) to yield the free amine of compound **2** (55.9 g, 39.2%) as a pale yellow oil.

2-[4-[2-(Benzimidazole-2-ylthio)ethyl]piperazin-1-yl]-*N*-(2,4-bis(methylthio)-6-methyl-3-pyridyl)acetamide hydrochloride (2) (K-604). The free amine of compound **2** (15.0 g, 29.8 mmol) and pyridine hydrochloride (6.90 g, 59.7 mmol) were dissolved in EtOH (25 mL) at the reflux temperature. This solution was added dropwise to boiling water (60 mL) at the reflux temperature over 2 min. The solvent (40 mL) was removed from the stirred solution by azeotropic distillation. The reaction mixture was allowed to cool to rt. The precipitated crystals were filtered out, rinsed with water (50 mL × 2) and dried over 80 ℃ under reduced pressure to

afford the title compound **2** (assigned the code **K-604**) as colorless fine needles (14.6 g, 88.6%). Mp 194-196 ℃; IR (KBr) cm^{-1}: 3431, 1674, 1625, 1564, 1520 ; ^{1}H-NMR (DMSO-*d6*) δ: 2.41 (3H, s), 2.44 (3H, s), 2.45 (3H, s), 3.04-3.10 (4H, m), 3.23-3.43 (8H, m), 3.70 (2H, t, *J* = 7.6 Hz) 6.89 (1H, s), 7.06-7.15 (2H, m), 7.40-7.51 (2H, m), 9.21 (1H, br s); ^{13}C-NMR (100 MHz, DMSO-*d6*) δ: 12.86, 14.16, 24.37, 26.79, 50.26 (2C), 51.45 (2C), 56.44, 59.92, 114.52 (2C), 114.96, 122.20 (2C), 125.18, 139.96 (2C), 149.52, 149.62, 156.54, 156.90, 167.85; Anal. Calcd for $C_{23}H_{30}N_6OS_2 \cdot HCl \cdot 0.9\ H_2O$: C, 49.74; H, 5.95; N, 15.13; Cl, 6.38; S, 17.32. Found: C, 49.97; H, 6.00; N, 15.24; Cl, 6.48; S, 17.26. HPLC purity: 99.50%. column: CAPCELPAK C18 UG120; column size 5 μm, 4.6 mm × 150 mm; mobile phase 10 mM SLS/5 mM H_3PO_4 : CH_3CN= 50 : 50; flow rate 1.0 mL/min; column temperature 40 °C; wavelength 247 nm; retention time 7.37 min.

2-[4-[2-(Benzoxazol-2-ylthio)ethyl]piperazin-1-yl]-*N*-(2,4-bis(methylthio)-6-methyl-3-pyridyl)acetamide (63). In a manner similar to that described for the free amine of compound **2,** compound **63** was prepared from **48** and **5** and recrystallized from AcOEt/*n*-hexane as colorless needles (83%). Mp 140-141 °C; IR (KBr) cm^{-1}: 3440, 3308, 2824, 1695, 1480; ^{1}H-NMR (DMSO-*d6*) δ: 2.43 (3H, s), 2.45 (3H, s), 2.47 (3H, s), 2.57-2.68 (6H, m), 2.80 (2H, t, *J* = 6.4 Hz), 2.86-2.91 (2H, m), 3.08 (2H, br s), 3.49 (2H, t, *J* = 6.4 Hz), 6.89 (lH, s), 7.25-7.36 (2H, m), 7.60-7.63 (2H, m), 8.77 (lH, br s); ^{13}C-NMR (100 MHz, DMSO-*d6*) δ: 11.66, 12.99, 23.17, 29.53, 51.70 (2C), 52.36 (2C), 55.85, 60.57, 109.24 , 113.74, 117.53, 123.36, 123.72, 124.20, 141.06, 148.21, 150.84, 155.12, 155.57, 163.99, 167.63; EIMS *m/z* 503 (M^+); Anal. Calcd for $C_{23}H_{29}N_5O_2S_3$: C, 54.84; H, 5.80; N, 13.90; S, 19.09. Found: C, 54.78; H, 5.84; N, 13.73; S, 19.01. HPLC purity: 99.57%. column: CAPCELPAK C18 UG120; column size 3 μm, 4.6 mm ×

100 mm; mobile phase 10 mM SLS/5 mM H_3PO_4 : CH_3CN : AcOH = 100 : 90 :1; flow rate 1.0 mL/min; column temperature 40 °C; wavelength 250 nm; retention time 9.26 min.

2-[4-[2-(Oxazolo[*4,5-b*]pyridin-2-ylthio)ethyl]piperazin-1-yl]-*N*-(2,4-bis(methylthio)-6-methyl-3-pyridyl)acetamide (65). In a manner similar to that described for the free amine of compound **2**, compound **65** was prepared from **48** and **54** as colorless needles (45%). Mp 119-121 °C; IR (KBr) cm^{-1}: 3448, 3274, 2816, 1699, 1493; ^{1}H-NMR (DMSO-*d6*) δ: 2.43 (3H, s), 2.45 (3H, s), 2.47 (3H, s), 2.56-2.67 (6H, m), 2.83 (2H, t, *J* = 6.8 Hz), 2.85-2.91 (2H, m), 3.08 (2H, br s), 3.54 (2H, t, *J* = 6.8 Hz), 6.89 (lH, s), 7.31 (1H, ddd, *J* = 8.2, 5.0, 1.4 Hz), 7.98 (1H, dd, *J* = 8.2, 1.4 Hz), 8.42 (1H, dd, *J* = 5.0, 1.5 Hz), 8.77 (lH, br s); ^{13}C-NMR (100 MHz, DMSO-*d6*) δ: 11.66, 13.00, 23.16, 29.71, 51.67 (2C), 52.34 (2C), 55.60, 60.55, 113.74, 116.85, 118.60, 124.20, 143.07, 145.02, 148.21, 155.01, 155.12, 155.57, 167.62, 168.39; EIMS *m/z* 504 (M^+); Anal. Calcd for $C_{22}H_{28}N_6O_2S_3$: C, 52.36; H, 5.59; N, 16.65; S, 19.06. Found: C, 52.37; H, 5.59; N, 16.62; S, 19.13. HPLC purity: 99.26%. column: CAPCELPAK C18 UG120; column size 5 μm, 4.6 mm ×150 mm; mobile phase 10 mM SLS/5 mM H_3PO_4 : CH_3CN= 50 : 50; flow rate 1.0 mL/min; column temperature 40 °C; wavelength 240 nm; retention time 5.63 min.

***In vitro* ACAT activity.**

Microsomal assay. ACAT activities were determined using arterial homogenates from New Zealand White (NZW) rabbits (Oriental Yeast Co.) fed a diet supplemented with 1% cholesterol (Wako Pure Chemical Industries) diet for 8 weeks and intestinal microsomes from normal NZW rabbits via the method of Heider et al. (*J. Lipid Res*., 1983, *24*, 1127-1134) with some modifications. The test compound was dissolved in DMSO (Dojindo Molecular Technologies) to yield the final desired concentrations (0.001, 0.01, 0.1, 1 and 10 μmol/L). The compound solution (2 μL) was added to 88 μL of 0.15 M phosphate buffer (pH 7.4) containing [^{14}C]-oleoyl-

CoA (Amersham International, 40 μM, 60,000 dpm) and bovine serum albumin (BSA) (Tissue Culture Biologicals, 2.4 mg/mL) complex and allowed to incubate at 37 °C for 5 min. After the microsomal suspension in phosphate buffer (10 μL) was added, the reaction mixture was incubated at 37 °C for 5 min (arterial) or 3 min (intestinal). The reaction was terminated by the addition of 3 mL of $CHCl_3$/MeOH (2:1) and 0.5 mL of 0.04 N HCl. After shaking, the organic layer was collected, and the solvent was evaporated. The extracted lipids were separated on a silica gel TLC plate (Merck) using a mixed solution of *n*-hexane/Et_2O/AcOH (75:25:1). The labeled cholesteryl oleate was detected by a BAS2000 (Fujifilm Corporation). The inhibitory activity was determined as the concentration at which the inhibitors reduced the formation of cholesteryl oleate by 50% (IC_{50}).

Cellular assay. J774A.1 cells (Dainippon Pharmaceutical Company) were cultured in Dulbecco's modified Eagle's medium (DMEM) (Sigma-Aldrich Company) containing 10% fetal bovine serum (FBS, Tissue Culture Biomedical) in a 24-well plate (Nalge Nunc International Corporation). The cells were incubated with a test compound dissolved in DMSO (5 μL) and 25-hydroxycholesterol (Sigma-Aldrich Company, 10 μg/mL) in 0.5 mL of the medium for 18 h. After removing the medium and washing twice with phosphate-buffered saline, lipids were extracted with 1.5 mL of *i*-PrOH/*n*-hexane (3:2). The extracts were dried, and the residues were dissolved in 0.2 mL of *i*-PrOH containing 10% Triton X-100 (Sigma-Aldrich Company). The FC and TC contents were measured by a Cholesterol E-test and a Free Cholesterol E-test (Wako Pure Chemical Industries), respectively. Proteins were solubilized with 0.25 mL of 2 N NaOH at 37 °C for 30 min and determined via the bicinchoninic acid (BCA) protein assay (Pierce). To calculate the CE contents, FC was subtracted from TC. The inhibitory activity was determined as the concentration at which the accumulation of CE was reduced by 50% (IC_{50}).

Pharmacokinetics. Compounds **2, 63** and **65** were orally administered to nonfasted Sprague-Dawley (SD) rats (male, 8 weeks old, n = 3) at a dose of 30 mg/kg in 0.05 N HCl solution. Blood samples (heparin plasma) were collected from the forearm vein 0.5, 1, 2, 4, 6 and 8 h after compound administration. NH_4OH (1.0 mL), the internal standard solution (0.2 mL, 1.0 μg/mL) and a mixed solvent (6 mL, ^{i}-PrOH/*n*-hexane = 5:95) were added to the plasma samples (0.2 mL). The resulting mixture was stirred for 10 min. The supernatant (organic layer) was collected and evaporated under a nitrogen stream. Then, the residue was dissolved in a mobile phase (0.2 mL, compound **2**: 0.1%HCOOH/MeOH/MeCN = 10:3:7; compound **63**: 0.1%HCOOH/MeOH/MeCN = 7:3:10; compound **65**: 0.1%HCOOH/MeOH/MeCN = 5:1:3). The concentrations of **2, 63** and **65** were measured via liquid chromatography/tandem MS (LC/MS). The MS was equipped with an electrospray ion source and operated in positive ion mode. The HPLC conditions were as follows: column, Symmetry RP8 (Waters) (3.0 mm × 150 mm); flow rate, 1.0 mL/min; and column temperature, 40 °C. Similarly, compound **2** was orally administered to male beagle dogs (n = 4) under fasting and nonfasting conditions at a dose of 10 mg/kg in 0.05 N HCl solution. Blood samples were collected from the foreleg veins 0.5, 1, 2, 4, 6 and 8 h after compound administration. The measurement procedures were conducted as described above.

***In vivo* study**. Male Bio F_1B hamsters (8 weeks old, Charles River Japan, Inc., Kanagawa, Japan) were used for the animal experiments. The animal room was controlled at 23±3 °C with relative humidity of 50±20%. The animals were fed a CE-2 chow diet (CLEA Japan Inc., Tokyo, Japan), followed by supplementation with CE-2 containing 0.3% cholesterol and 10% coconut oil for 10 weeks. During fat loading, **2** and **63** were added to the chow at 1, 3, 10, or 30 mg/kg/day whereas **65** was added to the chow at 3, 10, 30, or 100 mg/kg/day (*n*=7 for each dose

group). The reference compound, **CI-1011**, was added to the chow at 0.3, 1, 3, or 10 mg/kg/day (*n*=6 for each dose group). Blood samples were collected for the determination of plasma TC levels using a commercially available kit (Cholesterol E-Test Wako; Wako Pure Chemical Industries, Osaka, Japan). For atherosclerotic lesion analysis, the animals were anesthetized via an intraperitoneal injection of pentobarbital sodium (50 mg/kg) followed by vascular perfusion for 5 min with saline containing 4% paraformaldehyde with a perfusion pressure of 120 mm H_2O.

The aorta was separated from the heart at the upper portion 15 mm from the aortic origin. The isolated thoracic aorta was cut open, mounted on a rubber plate, fixed with 4% paraformaldehyde, and stained with oil red O. The lipid accumulation areas were measured with an image analysis system (SP500F; Olympus, Tokyo, Japan).

ASSOCIATED CONTENT

Supporting Information

Detailed experimental procedures for the syntheses of all compounds and their intermediates except **45**, **48**, **2**, **63** and **65** and the characterization data, HPLC purity, chemical stability test and chromosomal aberration test of **2**, **63** and **65**, and determination procedure for fp ratio of **2** in rabbit are provided in the Supporting Information. Molecular formula strings (CSV).

AUTHOR INFORMATION

Corresponding Author

*E-mail:k-sibuya@kowa.co.jp Phone:(+81) 42-391-6211. Fax: (+81) 42-395-0312.

ORCID

Kimiyuki Shibuya: 0000-0002-0027-5990.

Present Addresses

K. Kawamine: Research Strategy Department, Pharmaceutical Division, Kowa Company, Ltd., 3-4-14, Nihonbashihoncho, Chuoku, Tokyo 103-8433, Japan

T. Edano: Center for Interdisciplinary Cardiovascular Sciences, Brigham and Women's Hospital, Harvard Medical School, 3 Blackfan Cir, CLS, 17th Floor, Boston, MA 02115, USA.

Author Contributions

All authors have given approval to the final version of the manuscript and declare that they have no conflict of interest.

Notes

The authors declare no competing financial interest.

ACKNOWLEDGMENT

We thank Dr. Minoru Koura for conducting chemical stability test of compound **2**, **63** and **65**, and Ms. Noriko Inoue for performing the *in vitro* enzyme assays. We also acknowledge Dr. Masaya Iwashita for valuable discussions about pharmacology, and Drs. Gen Watanabe and Takaaki Araki for proof reading the manuscript

ABBREVIATIONS

ACAT, acyl-CoA:cholesterol *O*-acyltransferase; SARs, structure activity relationships; TC, total cholesterol; CE, cholesteryl ester; FC, free cholesterol; Tmax, maximum drug concentration time; Cmax, maximum drug concentration; AUC, area under the curve.

References

1. Stuckling, K. E.; Stange, E. F. Role of acy-CoA:cholesterol acyltransferase in cellular cholesterol metabolism. *J. Lipid. Res.* **1985**, *26*, 647-671.
2. Giovannoni, M. P.; Dal Piaz, V.; Vergelli, C.; Barlocco, D. Selective ACAT inhibitors as promising antihyperlipidemic, antiatherosclerotic and anti-Alzheimer drug. *Mini. Rev. Med. Chem.* **2003**, *3*, 576-584.
3. Alegret, M.; Llaverias, G.; Silvestre, J. S. Acyl Coenzyme A:cholesterol acyltransferase inhibitors as hypolipidemic and antiatherosclerotic drugs. *Methods Find Exp. Clin. Pharmacol.* **2004**, *26*, 563-586.
4. Ohshiro, T.; Tomoda, H. Isoform-specific inhibitors of ACATs: recent advances and promising developments. *Future Med. Chem.* **2011**, *3*, 2039-2061.
5. Ohshiro, T.; Tomoda, H. Acyltransferase inhibitors: a patent review (2010 – present). *Exp. Opin. Ther. Pat.* **2015**, *25*, 145-158.
6. Raal, F. J.; Marais, A. D.; Klepack, E.; Lovalvo, J.; McLain, R.; Heinonen, T. Avasimibe, an ACAT inhibitor, enhances the lipid lowering effect of atorvastatin in subjects with homozygous familial hypercholesterolemia. *Atherosclerosis* **2003**, *171*, 273-279.
7. Tardif, J-C. ; Grégorie, J.; L'Allier, P. L.; Anderson, T. J.; Bertrand, O.; Reeves, F.; Title, L. M.; Alfonso, F.; Schampaert, E.; Hassan, A.; McLain, R.; Pressler, M. L.; Ibrahim, R.; Lespérance, J.; Blue, J.; Heinonen, T.; Rodés-Cabau, J. Effects of the acyl coenzyme A:cholesterol acyltransferase inhibitor avasimibe on human atherosclerotic lesions. *Circulation* **2004**, *110*, 3372-3377.
8. Nissen, S. E.; Tuzcu, E. M.; Brewer, H. B.; Sipahi, L.; Nicholls, S. J.; Ganz, P.; Schoenhagen, P.; Waters, D. D.; Pepine, C. J.; Crowe, T. D.; Davidson, M. H.; Deanfield, J. E.; Wisniewski, L. M.; R. N.; Hanyok, J. J.; Kassalow, L. M. Effect of ACAT

inhibition on the progression of coronary atherosclerosis. *N. Eng. J. Med*. **2006**, *354*, 1253-1263.

9. Fazio, S.; Linton, M. Failure of ACAT inhibitor to retard atherosclerosis. *N. Eng. J. Med*. **2006**, *354*, 1307-1309.
10. Meuwese, M. C.; Groot, E.; Duivenvoorden, R.; Trip, M. D.; Ose, L.; Maritz, F. J.; Basart, D. C. G.; Kasterin, J. J.P.; Habib, R.; Davidson, M. H.; Zwinderman, A. H.; Schwocho, L. R.; Stein, E. A.; ACAT inhibition and progression of carotid atherosclerosis in patients with familial hypercholesterolemia. The CAPTIVATE randormized trial. *JAMA* **2009**, *301*, 1131-1139.
11. Meiner, V. L.; Cases, S.; Myers, H. M.; Sande, E. R.; Bellosta, S.; Schambelan, M.; Pitas, R. E.; McGuire, J.; Herz, J.; Farese, R. V. Disruption of the acyl-CoA:cholesterol acyltransferase gene in mice: evidence suggesting multiple cholesterol esterification enzymes in mammals. *Proc. Nat. Acad. Sci. U. S. A*. **1996**, *93*, 14041-14046.
12. Anderson, R. A.; Joyce, C.; Davis, M.; Reagan, J. W.; Clark, M.; Shelness, G. S.; Rudel, L. L. Identification of a form of acyl-CoA:cholesterol acyltransferase specific to liver and intestine in nonhuman primates. *J. Biol. Chem*. **1998**, *273*, 26747-26754.
13. Cases, S.; Novak, S.; Zheng, Y-W.; Myers, H. M.; Lear, S. R.; Sandc, E.; Welch, C. B.; Lusis, A. J.; Spencer, T. A.; Krause, B. R.; Erickson, S. K.; Farese, R. V. ACAT-2, a second mammalian acyl-CoA:cholesterol acyltransferase. Its cloning, expression, and characterization. *J. Biol. Chem*. **1998**, *273*, 26755-26764.
14. Oelkers, P.; Behari, A.; Cromley, D.; Billheimer, J. T.; Sturley, S. L. Characterization of two human genes encoding acyl coenzyme A:cholesterol acyltransferase-related enzymes. *J. Biol. Chem.* **1998**, *273*, 26765-26771.

15. Lee, O.; Chang, C. C. Y.; Lee, W.; Chang, T-Y. Immunodepletion experiments suggest that acyl-coenzyme A:cholesterol acyltransferase-1 (ACAT-1) protein plays a major catalytic role in adult human liver, adrenal grand, macrophages, and kidney, but not in intestines. *J. Lipid. Res*. **1998**, *39*, 1722-1727.

16. Lee, R. G.; Willingham, M. C.; Davis, M. A.; Skinner, K. A.; Rudel, L. L. Differential expression of ACAT1 and ACAT2 among cells within liver, intestine, kidney, and adrenal of nonhuman primates. *J. Lipid. Res*. **2000**, *41*, 1991-2001.

17. Temel, R. E.; Gebre, A. K.; Parks, J. S.; Rudel, L. L. Compared with acyl-CoA:cholesterol *O*-acyltransferase (ACAT)1 and lecithin:cholesterol acyltransferase, ACAT2 displays the greatest capacity to differentiate cholesterol from sitosterol. *J. Biol. Chem*. **2003**, *278*, 47594-47601.

18. Shibuya, Y.; Chang, C. C. Y.; Huang, L-H.; Bryleva, E. Y.; Chang, T-Y. Inhibiting ACAT1/ SOAT1 in microglia stimulates autophagy-mediated lysosomal proteolysis and increases Aβ1-42 clearance. *J. Neurosci*. **2014**, *34*, 14484-14501.

19. Yamanaka, K.; Urano, Y.; Takabe, W.; Saito, Y.; Noguchi, N. Induction of apoptosis and necroptosis by 24(S)-hydroxycholesterol is dependent on activity of acyl-CoA:cholesterol acyltransferase 1. *Cell Death Dis*. **2014**, *5*, e990.

20. Shibuya, Y.; Chang, C. C. Y.; Chang, T-Y. ACAT1/SOAT1 as a therapeutic target for Alzheimer's disease. *Future Med. Chem*. **201**5, *7*, 2451-2467.

21. Shibuya, K.; Watanabe, T.; Urano, Y.; Takabe, W.; Noguchi, N.; Kitagishi, H. Synthesis of 24(*S*)-hydroxycholesterol esters responsible for the induction of neuronal cell death. *Bioorg. Med. Chem*. **2016**, *24*, 2559-2566.

22. Takabe, W.; Urano, Y.; Vo, D-K. H.; Shibuya, K.; Tanno, M.; Kitagishi, H.; Fujimoto, T.; Noguchi, N. Esterification of 24S-OHC induces formation of atypical lipid droplet-like structures, leading to neuronal cell death. *J. Lipid. Res*. **2016**, *57*, 2005-2014.

23. Shibata, H.; Shibuya, K. An ACAT-1 inhibitor, K-604, ameliorates hepatic inflammation in NAFLD and NASH models. *Gastroenterol. Pancreatol. Liver Disord*. **2016**, *3*, 1-11.

24. Saraon, P.; Trudel, D.; Kron, K.; Dmitromanolakis, A.; Trachtenberg, J.; Bapat, B.; van der Kwast, T.; Jarvi, K. A.; Diamandis, E. P. Evaluation and prognostic significance of ACAT1 as a marker of prostate cancer progression. *Prostate* **2014**, *74*, 372-380.

25. Ohmoto, T.; Nishitsuji, K.; Yoshitani, N.; Mizuguchi, M.; Yanagisawa, Y.; Saito, H.; Sakashita, N. K604, a specific acyl-CoA:cholesterol 1 inhibitor, suppresses proliferation of U251-MG glioblastoma cells. *Mol. Med. Rep*. **2015**, *12*, 6037-6042.

26. Yang, W.; Bai, Y.; Xiong, Y.; Zhang, J.; Chen, S.; Zheng, X.; Meng, X.; Li, L.; Wang, J.; Xu, C.; Yan, C.; Wang, L.; Chang, C. C. Y.; Chang, T-Y.; Zhang, T.; Zhou, P.; Song, B-L.; Liu, W.; Sun, S-c.; Liu, X.; Li, B-l.; Xu, C. Potentiating the antitumour response of $CD8^+$ T cells by modulating cholesterol metabolism. *Nature* **2016**, *531*, 651-655.

27. Li, J.; Gu, D.; Lee, SS-Y.; Song, B.; Bandyopadhyay, S.; Chen, S.; Konieczny, S. F.; Ratliff, T. L.; Liu, X.; Xie, J.; Cheng, J-X. Abrogating cholesterol esterification suppresses growth and metastasis of pancreatic cancer. *Oncogene* **2016**, *35*, 6378-6388.

28. Shibuya, K.; Kawamine, K.; Sato, Y.; Miura, T.; Ozaki, C.; Edano, T.; Hirata, M. Novel Cyclic Diamine Compounds and Medicine Containing the Same. WO1998054153, May 26, 1998.

29. Shibuya, K.; Ohgiya, T.; Matsuda, T. Process for Producing Acid Adduct Salt of Polyacidic Base Compound. WO2004076441, Feb 27, 2004.

30. Ikenoya, M.; Yoshinaka, Y.; Kobayashi, H.; Kawamine, K.; Shibuya, K.; Sato, F.; Sawanobori, K.; Watanabe, T.; Miyazaki, A. A selective ACAT-1 inhibitor, K-604, suppresses fatty streak lesions in fat-fed hamsters without affecting plasma cholesterol levels. *Atherosclerosis* **2007**, *191*, 290-297.

31. Yoshinaka, Y.; Shibata, H.; Kobayashi, H.; Kuriyama, H.; Shibuya, K.; Tanabe, S.; Watanabe, T.; Miyazaki, A. A selective ACAT-1 inhibitor, K-604, stimulates collagen production in cultured smooth muscle cells and alters plaque phenotype in apolipoprotein E-knockout mice. *Atherosclerosis* **2010**, *213*, 85-91.

32. Shibuya, K.; Kawamine, K.; Miura, T.; Ozaki, C.; Edano, T.; Mizuno, K.; Yoshinaka, Y.; Tsunenari, Y. Design, synthesis and pharmacology of aortic-selective acyl-CoA cholesterol *O*-acyltransfersase (ACAT/SOAT) inhibitors. *Bioorg. Med. Chem.* **2018**, *26*, 4001-4013.

33. Kessler, H. Structure-activity relationships by NMR: A new procedure for drug discovery by a combinatorial-rational approach. *Angew. Chem. Int. Ed. Engl*. **1997**, *36*, 829-831.

34. Press, N. J.; Taylor, R. L.; Fullerton, J. D.; Tranter, P.; McCarthy, C.; Keller, T. H.; Arnold, N.; Beer, D.; Brown, L.; Cheung, R.; Christie, J.; Denholm, A.; Haberthuer, S.; Hatto, J. D. I.; Keenan, M.; Mercer, M. K.; Oakman, H.; Sahri, H.; Tuffnell, A. R.; Tweed, M.; Tyler, J. W.; Wagner, T.; Fozard, J. R.; Trifilieff, A. Solubility-driven optimization of phosphodiesterase-4 inhibitors leading to a clinical candidate. *J. Med. Chem*. **2012**, *55*, 7472-7479.

35. Guo, B.; Fan, H.; Xin, Q.; Chu, W.; Wang, H.; Huang, Y.; Chen, X.; Yang, Y. Solubility-driven optimization of (pyridin-3-yl)benzoxazinyloxazolidinones leading to a promising antibacterial agent. *J. Med. Chem*. **2013**, *56*, 2462-2650.

36. Fang, C.; Suemune, H.; Sakai, K. Chiral alcohol-induced diastereoselective conjugate addition and cyclization. *Tetrahedron Lett.* **1990**, *31*, 4751-4754.

37. Leysen, D.; Defert, O.; Alen, J.; Boland, S.; Bourin, A. P. J. Novel Rock inhibitors. WO2012146724, Apr 27, 2012.

38. Tashima, T.; Murata, H.; Kodama, H. Design and synthesis of novel and highly-active pan-histone deaceylase (pan-HDAC) inhibitors. *Bioorg. Med. Chem.* **2014**, *22*, 3270-3731.

39. Heider, J. G.; Pickens, C. E.; Kelly, L. A. Role of acyl CoA: cholesterol acyltransferase in cholesterol absorption and its inhibition by 57-118 in the rabbit. *J. Lipid. Res*. **1983**, *24*, 1127-1134.

40. Maduskuie, T. P.; Wilde, R. G.; Billheimer, J. T.; Cromley, D. A.; Germain, S.; Gillies, P. J.; Higley, C. A.; Johnson, A. L.; Pennev, P.; Shimshick, E. J.; Wexler, R. R. Design, synthesis, and structure-activity relationship studies for a new imidazole series of J774 macrophage specific acyl-CoA:cholesterol acyltransferase (ACAT) inhibitors. *J. Med. Chem.* **1995**, *38*, 1067-1083.

41. Trivedi, B. K.; Purchase, T. S.; Holmes, A.; Augelli-Szafran, C. E.; Essenburg, A. D.; Hamelehle, K. L.; Stanfield, R. L.; Bousley, R. F.; Krause, B. R. Inhibitors of acyl-CoA:cholesterol acyltransferase (ACAT). 7. Development of a series of substituted *N*-phenyl-*N'*-[(1-phenylcyclopentyl)methyl]ureas with enhanced hypocholesterolemic activity. *J. Med. Chem.* **1994**, *37*, 1652-1659.

42. Uchida, T.; Nakamura, E.; Usui, T.; Imasaki, H.; Kawakami, R.; Watanabe, T.; Higuchi, S. Disposition and metabolism of a novel diurea inhibitor of acyl CoA:cholesterol acyltransferas (YM17E) in the rat and dog. *Xenobiotica* **1994**, *24*, 1223-1236.

43. Nicolosi, R. J.; Wilson, T. A.; Krause, B. R. The ACAT inhibitor, CI-1011 is effective in the prevention and regression of aortic fatty streak area in hamsters. *Atherosclerosis* **1998**, *137*, 77-85.

44. Lee, H. T.; Sliskovic, D. R.; Picard, J. A.; Roth, B. D.; Wierenga, W.; Hicks, J. L.; Bousley, R. F.; Hamelehle, K. L.; Homan, R.; Speyer, C.; Stanfield, R. L.; Krause, B. R. Inhibitors of acyl-CoA:cholesterol *O*-acyl transferase (ACAT) as hypocholesterolemic agents. CI-1011: an acyl sulfamate with unique cholesterol-lowering activity in animals fed noncholesterol-supplemented diets. *J. Med. Chem.* **1996**, *39*, 5031-5034.

45. Ramharack, R.; Spahr, M. A.; Sekerke, C. S.; Stanfield, R. L; Bousley, R. F; Lee, H. T.; Krause, B. K. CI-1011 lowers lipoprotein(a) and plasma cholesterol concentrations in chow-fed cynomolgus monkeys. *Atherosclerosis* **1998**, *136*, 79-87.

46. Bocan, T. M. A.; Krause, B. R.; Rosebury, W. S.; Mueller, S. B.; Lu, X.; Dagle, C.; Major, T.; Lathia, C., Lee, H. The ACAT inhibitor Avasimibe reduces macrophages and matrix metalloproteinase expression in atherosclerotic lesions of hypercholesterolemic rabbits. *Arterioscler. Thromb. Vasc. Biol.* **2000**, *20*, 70-79.

47. Sorbera, L. A.; Rabasseda, X.; Castaňer, J. Avasimibe. *Drugs Fut.* **1999**, *24*, 9-15.

48. Rodriguez, A.; Usher, D. C. Anti-atherogenic effects of the acyl-CoA:cholesterol acyltransferase inhibitor, avasimibe (CI-1011), in cultured primary human macrophages. *Atherosclerosis* **2002**, *161*, 45-54.

49. Llaverias, G.; Laguna, J. C.; Alegret, M. Pharmacology of the ACAT inhibitor Avasimibe (CI-1011). *Cardiovasc. Drug Rev*. **2003**, *21*, 33-50.

50. McKenney, J. M. Pharmacological charcteristics of statins. *Clin. Cardiol.* **2003**, *26 (suppl. III)*, 32-38.

51. Catapano, A. L. Pitavastatin:a different pharmacological profile. *Clin. Lipidol.* **2012**, *7 (suppl.1),* 3-9.

52. Vargo, R.; Adewale, A.; Behm, M. O.; Mandema, J.; Kerbusch, T. Prediction of clinical irrelevance of PK differences in atorvastatin using PK/PD models derived from literature-based meta-analyses. *Clin. Pharmacol. Ther.* **2014**, *96*, 101-109.

53. Urano, Y.; Noguchi, N.; Shibuya, K.; Morikawa, S. Nasally administered medical composition. WO2018092765, Nov 14, 2017. In our patent information, we disclosed data of PK (K-604 drug concentration) and PD (lipid modulation) in the brains of mice. In the intranasal administration of K-604 (108 μg) to mice, the drug concentration (Cmax 37.8 ng/g) in the brain soon disappeared in a few hours, as shown in Figure 4 of the patent. Even with a single daily dose for 7 days, the proportion of CE/FC (the level of CE was decreased from 0.70 μmol/g to 0.04 μmol/g) and 24(*S*)-hydroxycholesterol (the level was increased from 5.16 μmol/g to 5.36 μmol/g) could be significantly altered as a result of the ACAT-1 inhibitory effect, as shown in Figures 5 and 6 of the patent. Based on these results, we draw the conclusion that ACAT-1 inhibition in the aorta can be dominated by Cmax or transitory drug exposure, but not by AUC or long drug exposure after intranasal administration.

54. Robertson, D. G.; Breider, M. A.; Milad, M. A. Preclinical safety evaluation of Avasimibe in beagle dogs: an ACAT inhibitor with minimal adrenal effects. *Toxicol. Sci.* **2001**, *59*, 324-334.

55. Tanaka, A.; Terasawa, T.; Hagihara, H.; Ishibe, N.; Sawada, M.; Sakuma, Y.; Hashimoto, M.; Takasugi, H.; Tanaka, H. Inhibitors of acyl-CoA:cholesterol *O*-acyltransferase. 3.

Discovery of a novel series of *N*-alkyl-*N*-[(fluorophenoxy)benzyl)-*N'*-arylureas with weak toxicological effects on adrenal glands. *J. Med. Chem.* **1998**, *41*, 4408-4420.

56. Dominick, M. A.; McGuire, E. J.; Reindel, J. F.; Bobrowski, W. F.; Bocan, T. M. A.; Gough, A. W. Subacute toxicity of a novel inhibitor of acyl-CoA:cholesterol acyltransferasc in beagle dogs. *Fundam. Appl. Toxicol*. **1993**, *20*, 217-224.
57. Dominick, M. A.; Bobrowski, W. A.; MacDonald, J. R.; Gough, A. W. Morphogenesis of a zone-specific adrenocortical cytotoxicity in guinea pigs administered PD 132301-2, an inhibitor of acyl-CoA:cholesterol acyltransferase. *Toxicol. Pathol*. **1993**, *21*, 54-62.
58. Vernetti, L. A.; MacDonald, J. R.; Wolfgang, G. H. I.; Dominick, M. A.; Pegg, D. G. ATP depletion is associated with cytotoxicity of a novel lipid regulator in guinea pig adrenocortical cells. *Toxicol. Appl. Pharm*. **1993**, *118*, 30-38.
59. Reindel, J. F.; Dominick, M. A.; Bocan, T. M. A.; Gough, A. W.; McGuire, E. J. Toxicologic effects of a novel acyl-CoA:cholesterol acyltransferase inhibitor in cynomolgus monkeys. *Toxicol. Pathol*. **1994**, *22*, 510-518.
60. With a similar correction, the aortic IC_{50} value (33 nM and 120 nM) of **63** and **65** decreased to 0.89 nM and 3.24 nM, respectively. Accordingly, the isoform selectivities are 33-fold and 65-fold, respectively. We presumed that the longest $T_{1/2}$ (10.1 h) and largest AUC (4125 ng·h/mL) of **63** with a potent intestinal IC_{50} value (29 nM) contributed to act on the intestine during a long duration and remarkably lowered TC despite showing 33-fold isoform selectivity. Although compound **65** exhibited a relatively large AUC, it showed a short $T_{1/2}$ (3.4 h) and a relatively weak IC_{50} value (210 nM) for intestinal ACAT (or ACAT-2) compared to **63** (29 nM). Although the isoform selectivity is generally acceptable to explain the difference in pharmacological outcome,

the pharmacodynamics (PD) effect can be dominated not only by isoform selectivity as a single parameter but also by complicated PK parameters such as $T_{1/2}$ and AUC. After all, PK/PD model of **2**, **63** and **65** are well-displayed as featured profiles in Figure 6.

61. Libby, P.; Aikawa, M. Stabilization of atherosclerotic plaques: New mechanisms and clinical targets. *Nat. Med.* **2002**, *8*, 1257-1262.

62. In the Phase II study (https://clinicaltrials.gov/ct2/show/NCT00851500?term=K-604&rank=1), our plans were to set up safety assessments including the ACTH stimulation test, and to measure the carotid plaque composition (lipid rich/necrotic core) as a primary efficacy endpoint and the carotid plaque size as a secondary efficacy endpoint by Magnetic Resonance Imaging after 26 weeks when rosuvastatin was administered to all patients, who were composed of a placebo group, a low-dose K-604 group and a high-dose K-604 group. The lipid profiles (LDL-C) of all patients were lowered well below the average range between 70 and 90 mg/dL by add-on therapy with rosuvastatin.

Insert Table of Contents artwork here

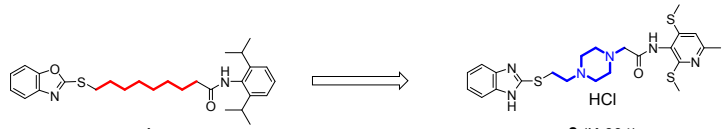

1

Rabbit aortic ACAT IC_{50} = 0.004 μM
Rabbit intestinal ACAT IC_{50} = 0.021 μM
cLogP 7.25
Aqueous solubility 0.03 μg/mL at pH 1.2

HCl

2 (K-604)

Rabbit aortic ACAT IC_{50} = 0.084 μM
Rabbit intestinal ACAT IC_{50} = 0.45 μM
Human ACAT-1 IC_{50} = 0.45 μM
Human ACAT-2 IC_{50} = 102.85 μM
LogP 3.3 at pH 6.8
Aqueous solubility 19 mg/mL at pH 1.2

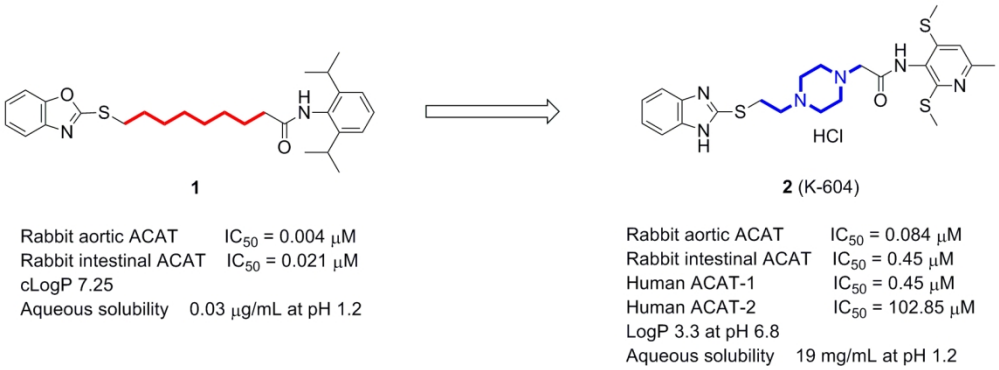

Table of Contents

153x57mm (300 x 300 DPI)